Title: Early Neoproterozoic metagabbro-tonalite-trondhjemite of Sør Rondane (East Antarctica): implications for supercontinent assembly

Author: Marlina Elburg Joachim Jacobs Tom Andersen Chris Clark Andreas Läufer Antonia Ruppel Nicole Krohne Detlef Damaske

PII: S0301-9268(14)00369-6
DOI: http://dx.doi.org/doi:10.1016/j.precamres.2014.10.014
Reference: PRECAM 4120

To appear in: *Precambrian Research*

Received date: 6-3-2014
Revised date: 1-10-2014
Accepted date: 15-10-2014

Please cite this article as: Elburg, M., Jacobs, J., Andersen, T., Clark, C., Läufer, A., Ruppel, A., Krohne, N., Damaske, D.,Early Neoproterozoic metagabbro-tonalite-trondhjemite of Sor Rondane (East Antarctica): implications for supercontinent assembly, *Precambrian Research* (2014), http://dx.doi.org/10.1016/j.precamres.2014.10.014

Highlights:

The ca. 1 Ga meta-igneous rocks of the Sør Rondane Mountains (E. Dronning Maud Land, Antarctica) were generated in an oceanic arc setting

Subduction halted around 950 Ma, giving rise to more diverse magmatism

Igneous ages and isotopic characteristics suggest a pre-Gondwana connection to India-Sri Lanka - Madagascar

Early Neoproterozoic metagabbro-tonalite-trondhjemite of Sør Rondane (East Antarctica): implications for supercontinent assembly

Marlina Elburg[1,2], Joachim Jacobs[3,4], Tom Andersen[5], Chris Clark[6], Andreas Läufer[7], Antonia Ruppel[7], Nicole Krohne[8], Detlef Damaske[7]

[1]Discipline of Geology, SAEES, UKZN, Westville, South Africa

[2]Department of Geology, University of Johannesburg, PO Box 524, Auckland Park 2006, South Africa, marlinae@uj.ac.za

[3]Department of Earth Science, University of Bergen, Allégaten 41, 5007 Bergen, Norway

[4]Norwegian Polar Institute, Fram Centre, 9296 Tromsø, Norway

[5]Department of Geosciences, University of Oslo, Norway

[6]Department of Applied Geology, Curtin University, GPO Box U1987, Perth, WA 6845, Australia

[7]Federal Institute of Geosciences and Natural Resources (BGR), Stilleweg 2, 30655 Hannover, Germany

[8]Department of Geosciences, University of Bremen, PF 330 440, 28334 Bremen, Germany

1. Abstract

New data for intrusive meta-igneous rocks from the Southwest terrane of the Sør Rondane Mountains confirm the view that this is a juvenile oceanic arc terrane, with the main phase of subduction-related magmatic activity around 995-975 Ma. Younger magmatism (960-925 Ma) is more varied: a high Sr/Y ('adakitic') suite is

present, as well as high-Ti mafic dykes, and one sample of A-type granite. This is interpreted as reflecting the end of subduction. The occasional presence of Archaean inherited zircons suggests proximity of Sør Rondane to an older continental nucleus from which detritus was shed. Although the 'meta-igneous sector' appears to be unique in representing a juvenile oceanic arc terrane, igneous ages and isotopic compositions around 1000-900 Ma suggest a broad coherence between outcrops ranging from Schirmacher Oasis (11 degrees E) to Yamato Mts (35 degrees E). This area seems unrelated to the slightly older, and isotopically and geochemically more enriched Mesoproterozoic rocks of central and western Dronning Maud Land. A closer relation appears to exist with Sri Lanka-India-Madagascar during the earliest Neoproterozoic than with southern Africa.

2. Introduction

The Sør Rondane Mountains, located in the eastern part of Dronning Maud Land, have been subjected to an appreciable amount of geological research recently, as they have been proposed to lie in an area where several fold belts, related to the amalgamation of Gondwana, interact (Boger, 2011; Jacobs et al., 1998; Meert, 2003; Osanai et al., 2013). To correctly interpret Gondwanan events it is important to characterise the fragments involved in amalgamation, and their similarities and distinctions to neighbouring areas. In this context, interesting differences between the ca. 1 Ga meta-igneous samples from Sør Rondane and those from the more westerly parts of Dronning Maud Land were noted recently (Kamei et al., 2013; Owada et al., 2013; Shiraishi et al., 2008).

With the present contribution, we want to add to the data and discussion provided by previous authors on the 1.0-0.9 Ga meta-igneous rocks (the 'metatonalite suite' of

Kamei et al., 2013) in the southwestern part of Sør Rondane. We will focus on the integration of zircon U-Pb, Lu-Hf and trace element data with whole rock geochemical data to assess the models proposed for the tectonic setting in which the magmas were generated. A comparison with data from neighbouring areas in Antarctica and its Gondwana neighbours will be used to assess the tectonic implications for the Rodinia as well as Godwana supercontinent.

3. Geological Background

The first geological investigations of the Sør Rondane Mountains were carried out by Belgian expeditions in the 1950-60s, who recognised that an older series of metamorphic rocks (metatonalites and related lithologies) was intruded by younger (now known to be Pan-African) granites (Van Autenboer et al., 1964). More recent mapping has been done by Japanese expeditions, who also published a geological map of the area (Shiraishi et al., 1997), and whose most recent efforts were described in a special issue of Precambrian Research (volume 234, 2013).

The Sør Rondane Mountains have been divided into two areas of different metamorphic affinities, the granulite-amphibolite-facies Northeast (NE) terrane and amphibolite-greenschist-facies Southwest (SW) terrane. The boundary between the two areas, first named the 'Sør Rondane Suture' (Shiraishi et al., 1997) has recently been redefined as the 'Main Tectonic Boundary' (Osanai et al., 2013), and shifted slightly northwards compared to its location inferred previously. What will be referred to as the ‘meta-igneous sector’ is part of the SW-terrane, located between the Main Shear Zone (MSZ; with a dextral sense of shear (Ruppel, 2012)) in the north and another, inferred, shear zone north of Dufekfjellet in the south (Fig. 1), where the rocks consist almost wholly of meta-igneous rocks, at amphibolite-greenschist facies.

The part of the SW-terrane located north of the MSZ consist largely of metasedimentary, rather than meta-igneous rocks, and has experienced granulite- to amphibolite-facies metamorphism (Osanai et al., 2013).

Data on the meta-igneous suite have been provided by the reports to the individual geological maps of Sør Rondane (Shiraishi et al., 1992), and by Ikeda and Shiraishi (1998), but a more detailed study was done by Kamei et al. (2013), and additional data, focussed on the mafic end member, were presented by Owada et al. (2013). The work by Kamei et al. (2013) divides the area in several suites: a 998-995 Ma (SHRIMP U-Pb zircon) gneissose Bt-Hbl metatonalite, with tholeiitic affinities in terms of (elevated) FeO*/MgO ratios, with associated mafic enclaves; and four suites of calc-alkaline rocks (hbl-bt metatonalite, hbl metagabbro, hbl-bt tonalitic gneiss, and bt metatonalite), which yielded ages of 945-920 Ma, apart from a sample of bt metatonalite in Nils Larsenfjellet, which gave an age of 772 Ma. On the basis of the geochemical characteristics of the two suites, Kamei et al. (2013) proposed a juvenile oceanic arc setting for the tholeiitic suite, and interpreted the calc-alkaline suite as having formed by an 'adakite scenario', i.e. melting of a subducted oceanic slab with residual garnet, also in a subduction setting.

In contrast, Owada et al. (2013) focussed on the mafic rocks associated within the meta-igneous sector, and divided them into a ca. 995 Ma low-Ti (TiO_2<1.2 wt.%) suite of mafic enclaves and a ca. 945 Ma high-Ti (TiO_2>1.2 wt.%) suite of dykes. Owada et al. (2013) also interpreted the low-Ti samples to have formed in a juvenile arc terrane, but the younger, high-Ti group was, interpreted to have been formed in a back-arc setting, contrasting with the subducted slab-melt scenario of Kamei et al. (2013).

4. Sample Description

4.1. Field appearance

A total of thirty-four samples was collected from the outcrops occurring to the south of the 'Main Shear Zone' (Shiraishi et al., 1997; Fig. 1) during the German-led 'Geodynamic Evolution of East Antarctica' (GEA) expeditions I and II in the Austral summer of 2010-2011 and 2011-2012. The rocks are dominantly coarse-grained and mesocratic in appearance, with a distinctly green tinge. More melanocratic rocks can be fine- or coarse-grained. The melanocratic rocks occur as discrete mappable bands or as mafic enclaves or dykes within the more mesocratic rocks (Fig. 2a-f). In some cases, the mafic enclaves can be seen to originate from mafic dykes. Leucocratic dykes of up to 5 meters width have also been observed. There is plenty of evidence of ductile deformation in the field, especially close to the 'Main Shear Zone', but the intensity of this deformation is variable. In some instances, it is possible to recognise textures that can be interpreted to be of igneous origin, such as the presence of (subvolcanic) quartz phenocrysts (Fig. 3a) and larger feldspar crystals that are likely to have been phenocrysts before becoming porphyroclasts.

4.2. Petrography

All samples analysed are, essentially, metamorphic rocks, with epidote and chlorite as the most obvious metamorphic minerals, but the extent to which they have been metamorphosed is variable. In some samples, plagioclase crystals are wholly replaced by finer-grained epidote, while in other samples igneous oscillatory zoning may still be visible within the plagioclase (Fig. 3b).

Because of the metamorphic overprint, the samples have been classified (Fig. 4) on the basis of their normative mineralogy and intrusive QAPF classification (Le Maitre,

2002), with the additional category of trondhjemite based on the Ab-An-Or diagram of Barker (1979) (see Geochemistry section, and Electronic Appendix 2, which also gives data on the modal mineralogy).

The texture of the meta-(quartz-)gabbros is variable: it can be foliated, porphyroclastic, coarse-or fine-grained equigranular, meta-porphyritic, meta-ophitic, or poikilitic, with large oikocrysts of amphibole. In some cases, amphibole is zoned from cores with a more olive-green colour to rims where the green has a more bluish tinge. Plagioclase in variable stages of epidotisation is present in all samples, as is minor quartz. Chlorite is more common in the sheared samples. Opaque minerals are present in most samples, and titanite in some. Apatite is an accessory phase, apart from sample MESR109, in which it occurs at the percent level; this sample also contains more abundant oxides than other meta-gabbros.

Intermediate samples mainly classify as metatonalites, and contain lower modal amounts of amphibole, while chlorite and quartz increase in abundance, with biotite in more potassium-rich samples. Accessory minerals are apatite, zircon, titanite, and opaque minerals, and more rarely rutile. In some samples, the opaque minerals are partially replaced by titanite. Amphibole is sometimes riddled with small inclusions of opaque minerals and/or rutile, often elongated in certain orientations with respect to the host crystal, suggesting they were formed by exsolution. Garnet occurs as eu- to subhedral crystals in samples with higher FeO*/MgO ratios. It can contain inclusions of opaque minerals, and does not display reaction rims; it is therefore interpreted to be formed during prograde metamorphism of the tonalites. Calcite occurs as a secondary mineral in some samples. Sample MESR99 classifies as a tonalite, but is extremely low in mafic minerals (leucotonalite).

The metatrondhjemites mainly differ from the metatonalites in their lower modal amount of amphibole, the absence of titanite and higher quartz contents, but the distinction between tonalite (modal An%>30) and trondhjemite (modal An%<30) is gradual.

One sample (MESR49a) is an only slightly metamorphosed quartz-monzodiorite, and, unlike all the other samples, contains microcline. Samples MESR97, 105 and 106 are classified as metagranodiorites, and contain white mica.

All samples show some signs of deformation, varying from undulose extinction of the quartz, to sutured grain boundaries and a porphyroclastic texture, whereby larger plagioclase crystals are enveloped by ribbons of quartz, amphibole, epidote and chlorite defining an S-C fabric. Neither the intensity of metamorphism, as evidenced by the extent of epidote formation, nor the intensity of deformation appears to be related to the age (varying between ca. 1015 and 925 Ma, see below) of the samples.

5. Analytical Techniques

A more detailed description of the analytical techniques used is given in Electronic Appendix 1. Major and trace elements were analysed at the Discipline of Geological Sciences, University of KwaZulu-Natal, by X-ray Fluorescence (XRF) Spectrometry on fused discs and pressed pellets respectively, using a Panalytical Axios–minerals sequential XRF spectrometer. Lower-level trace elements were analysed by laser ablation (LA) inductively coupled plasma mass spectrometry (ICPMS) of the XRF

fused discs using an NWR UP-213 laser and Perkin-Elmer Nexion quadrupole ICPMS. Trace elements in zircon were also analysed using the latter set-up.

Laser-ablation U-Pb and Lu-Hf isotopic analyses were performed at the Department of Geosciences, Oslo University, using an NWR UP-213 laser and a Nu Instruments multi-collector ICPMS, following techniques described by Elburg et al. (2013). Four samples were dated by U-Pb on zircon using a Sensitive High Resolution Ion-Microprobe (SHRIMP) at Curtin University (Perth, Western Australia; Electronic Appendix 1). Two samples were analysed for Sr and Nd isotopes at the Department of Geological Sciences of the University of Cape Town.

6. Zircon U-Pb and Lu-Hf data

Zircon U-Pb data were acquired on a total of twelve samples, spanning the geographic area from which the samples were obtained. Eight of these were analysed by LA-MC-ICPMS (sample identifiers starting with 'MESR') and four by SHRIMP (sample identifiers starting with a number). The full data set can be found in Electronic Appendix 2. All uncertainties are quoted at the 2-sigma level.

The zircons that were dated by LA-ICPMS were also analysed for their Lu-Hf isotope systematics to determine the initial $^{176}Hf/^{177}Hf$ ratios and assess the degree of homogeneity within the samples.

Sample 07c1 comes from a mesoscopically undeformed tonalite, containing abundant mafic enclaves (Fig. 2e). This locality is ca. 1 km S of the MSZ (Fig. 1). The up to 400 µm large zircons are clear to light brownish with few inclusions. In cathodoluminescence (CL) imaging, zircons show irregular sector zoning, and

sometimes a faint oscillatory zoning. Eighteen spots were analysed on eighteen crystals. Typical U-concentrations range from 100-900 ppm (Th/U: 0.15-0.28). The 18 analyses define a concordia age of 986 ± 3 Ma (Fig. 5a), which is interpreted as the crystallisation age of the tonalite. This is indistinguishable of the weighted average $^{207}Pb/^{206}Pb$ age of 987 ± 6 Ma.

Sample 07a1 represents the mylonite equivalent of the metatonalite (Fig. 2f), as exposed in the southern part of the MSZ, west side of Yuboku Valley (Fig. 1). It contains zircons that appear as anhedral fragments up to 200 µm in size. Zircons are clear to light brownish and have numerous inclusions. In CL images, they show oscillatory or sector zoning. Some zircons have high-U rims, which are too thin to be analysed. Eighteen crystals were analysed with one spot each. The zircons are low in U (70-210 ppm) with Th/U from 0.13-0.24. Two spots yielded discordant ages, and one spot gave an age that was c. 50 Ma younger than the other analyses. The remaining fifteen analyses yielded a concordia age of 979 ± 5 Ma (Fig. 5b), which is interpreted to be the age of the tonalitic protolith to the mylonite. The weighted average $^{207}Pb/^{206}Pb$ age is similar at 987 ± 13 Ma The discordant analyses probably reflect Pb-loss as the result of deformation.

Sample 12b4 comes from the east side of Widerøefjellet and is a heterogeneous, fine-grained felsic gneiss of trondhjemitic composition. The zircons are mostly small and clear, often not exceeding 100 µm in size. In CL imaging, the zircons show moderate zoning. Some zircons have metamict cores others have thin high-U rims. Sixteen grains were analysed from the main weakly oscillatory-zoned parts, which have typical U concentrations of 250-500 ppm (Th/U: 0.36-0.48). Fourteen analyses

define a concordia age of 984 ± 6 Ma (Fig. 5c), albeit with a slightly high MSWD of concordia of 4.5. This age is the best estimate of the igneous crystallisation age of the sample, and within error of the weighted average $^{207}Pb/^{206}Pb$ age of 994 ± 8 Ma. The remaining four analyses can be used to give a discordia with a very poorly defined lower intercept and an upper intercept of 1024 ± 14 Ma (weighted average $^{207}Pb/^{206}Pb$ age is 1039 ± 13 Ma). The MSWD of this discordia is 0.58, and its relevance will be discussed in conjunction with the LA-MC-ICPMS data for sample MESR99 from the same general area.

Sample 28b2 comes from an area to the northwest of 12b4 and is a foliated metatonalite. The zircons are stubby, light brownish and mostly anhedral. In CL, the zircons show a core-rim relationship, with dark cores and very bright irregular rims. Twelve crystals were analysed, targeting eight cores and 4 rims. One core yielded a strongly discordant analysis. Whilst the high-U cores have U from 500-2200 ppm (Th/U: 0.14-0.52), the rim analyses have much lower U ranging from 60-150 ppm (Th/U: 0.38-0.41). However, the seven core and four rim analyses are indistinguishable in age and yield a concordia age of 991 ± 5 Ma (Fig. 5d), which is interpreted as the crystallisation age of the protolith, indistinguishable from the weighted average $^{207}Pb/^{206}Pb$ age of 990 ± 6 Ma.

Sample MESR99 comes from an area between 12b4 and 28b2 on the east side of Widerøefjellet (Fig. 1, 2b). The outcrop consists of a variety of undeformed rock types, ranging from mesocratic to leucocratic metatonalite. The most mafic compositions are represented as mafic enclaves within an intermediate fairly coarse-grained intrusive. The most leucocratic material is present as 10 m-sized semi-

angular patches with equidimensional to elongate shapes. The geological relationships between the different phases is unclear from field observations, as no chilled contacts were observed. The dated sample is of the leuco-tonalite, which is homogeneously fine-grained. Its zircons are euhedral, with aspect ratios <2:1 and typically only 100-150 µm in their longest dimension. Many of them have a turbid brown appearance, but clear ones are found as well. Back-scattered electron (BSE) imaging shows that some zircons display well-defined oscillatory zoning (Fig. 5e), but others have more patchy zoning; the latter crystals typically yielded discordant analyses with significant common Pb. Many zircons have a thin, darker rim, which was not of sufficient size to be analysed. Thirty-six crystals were analysed, and yielded U-contents of 600-1200 ppm, with Th/U ratios (determined by LA-Q-ICPMS) of 0.4-1. Sixteen analyses yielded discordant and/or common-Pb influenced analyses. The remaining twenty analyses had $^{206}Pb/^{204}Pb$ ratios > 8,000 and yielded a concordia age of 1015 ± 4 Ma, with an MSWD of 4.3 (weighted average $^{207}Pb/^{206}Pb$ age is 1010 ± 5 Ma). The somewhat high MSWD reflects a range in the ages of the individual points between 1031 and 998 Ma (Fig. 5e). The homogeneity in crystal size and shape, and their oscillatory zoning indicates that this is a single population of igneous zircons, and the age is interpreted to be the crystallisation age of the zircons. A similar age is found from the discordia of four zircons in sample 12b4, from slightly further north. However, the main igneous age there is younger at 984 ± 6 Ma. This may reflect a next phase of magmatism, which may also have been responsible for the (undated) thin rims on the zircons in MESR99.

The average initial $^{176}Hf/^{177}Hf$ ratio of the 29 zircons analysed is 0.282334 ± 0.000089 (2 sigma; fig. 6). The scatter is slightly outside that expected from analytical uncertainty, based on the repeated analyses of the Temora standard. The

two lowest analyses might be outliers, and if these are left out the average comes to 0.282341 ± 0.000074, which translates to an εHf_i of 6.5 ± 2.6.

Sample MESR43 was taken near the bottom of a traverse down the south-central part of Widerøefjellet (Fig. 1), and it is a moderately deformed, coarse-grained metatonalite. Its zircons are generally clear, with a light-purple colour and aspect ratios <2:1. Their size is around 200-350 µm. Zoning is only poorly visible in BSE images, but appears to be oscillatory (Fig. 5f). Twenty-six crystals (with U concentrations of 200-500 ppm; Th/U ratios around 0.25) were analysed, of which only one is discordant. The other twenty-five analyses define a concordia age of 991 ± 4 Ma, albeit with a slightly elevated MSWD of 2.5. This age is within error of the weighted average $^{207}Pb/^{206}Pb$ age of 986 ± 4 Ma, and is interpreted as the crystallisation age of the intrusion.

The twenty-six Lu-Hf analyses constitute a homogeneous population, with the spread in data within that expected from analytical uncertainty. The average initial $^{176}Hf/^{177}Hf$ ratio is 0.282360 ± 0.000056, or εHf_i of 6.5 ± 2.0.

Sample MESR104 comes from Nils Larsenfjellet and is a moderately deformed metatonalite, which in places contains mafic enclaves. Zircons in this sample are about 200 µm and have aspect ratios from 1:1 to 3:1. Cathodoluminescence (CL) imaging shows well-defined oscillatory zoning in most crystals. Nineteen grains (U contents 200-600 ppm, Th/U=0.25-0.5) were ablated, of which five gave discordant analyses. The other fourteen gave a concordant age of 986 ± 6 Ma (Fig. 5g;

weighted average $^{207}Pb/^{206}Pb$ age is 984 ± 7 Ma), with an MSWD of 0.15, and this age is most likely to reflect the igneous crystallisation age of the sample.

Twenty zircons yielded a homogeneous Hf isotope population with an initial $^{176}Hf/^{177}Hf$ ratio of 0.282353 ± 0.000049, or εHf_i of 6.3 ± 1.7.

Sample MESR79 is a coarse-grained metatrondhjemite from Bamseungen. Its zircons are between 100 and 200 µm, with aspect ratios up to 3:1, and show oscillatory zoning, which is poorly defined in BSE images, but clearly visible in CL. Some featureless cores are present too. Twenty-five ablations were performed on 23 grains. U concentrations were variable, from 50-200 ppm, but with spikes up to 3000 ppm; Th/U ratios were 0.4-1, with the higher values for the U-enriched grains. Some grains caused problems, because of elevated count rates for ^{206}Pb (>1 Mcps) causing dead-time problems and deviation from ion-counter linearity, resulting in reversely discordant analyses. Only fifteen analyses could therefore be used to obtain the igneous age of this sample, which is a concordia age of 986 ± 7 Ma (MSWD = 0.2; Fig. 5h), within error of the weighted average $^{207}Pb/^{206}Pb$ age of 990 ± 18 Ma.

Twenty-seven zircons were analysed for Lu-Hf systematics, of which two gave values that were significantly lower than the main population, and the CL image of one of these zircons showed the presence of a core, with a slightly discordant $^{207}Pb/^{206}Pb$ age of 1043 ± 32 Ma. Without these two analyses, the average initial $^{176}Hf/^{177}Hf$ ratio is 0.282380 ± 0.000067, or εHf_i of 7.3 ± 2.4.

Sample MESR106 was taken from the southeastern side of Widerøefjellet in an area with both felsic and mafic intrusives. It is a fine-grained granodiorite, with zircons of 100-200 µm. They are euhedral with aspect ratios from 2:1 to 5:1, and show concentric zoning, generally mimicking the outline of the crystal, in BSE images. Slightly brighter cores, with cracks around them, are present in some crystals. Twenty-six spots were ablated, with U contents typically 200-800 ppm, and Th/U between 0.25 and 0.45. One crystal gave an age of c. 3 Ga, and four crystals yielded ages of 1050-995 Ma. Eleven other analyses gave concordant analyses, which together defined an age of 957 ± 8 Ma (Fig. 5i; weighted average $^{207}Pb/^{206}Pb$ age is 957 ± 5 Ma), which is likely to be the crystallisation age of the intrusion.

The igneous population (n=21) gave an initial $^{76}Hf/^{177}Hf$ ratio of 0.282406 ± 0.000059, or εHf_i of 7.5 ± 2.1. The four grains that are slightly older give a marginally lower initial $^{76}Hf/^{177}Hf$ ratio of 0.282374 ± 0.000049. The initial $^{176}Hf/^{177}Hf$ ratio of the ca. 3 Ga grain was 0.28096 ± 0.000028 or εHf_i of 3.6 ± 0.9.

Sample MESR49a comes from the southernmost nunatak of the Lågkollane group, which consists of moderately deformed coarse-grained quartz-monzodiorite, intruded by undeformed finer-grained granitoid and a pegmatite dyke. The sample is of the deformed quartz-monzodiorite. It contains numerous euhedral zircons between 200 and 400 µm in length and aspect ratios around 3:1. Cracks and inclusions are quite common. Several contain cores that are very bright and patchy in BSE images, but the majority of crystals displays fine-scale oscillatory zoning. Thirty-six spots were analysed, but many of them were discordant and rich in common Pb, probably as a result of the many cracks and inclusions. U contents are 200-500 ppm, and Th/U

ratios around 0.35. Only twelve analyses were of sufficient quality to be retained, and ten of these yielded a concordia age of 947 ± 8 Ma (Fig. 5j). However, since most analyses plotted below the concordia, the MSWD of concordance is as high as 14. A discordia through the same sample set gives an upper intercept of 968 ± 21 Ma, which is within error of the concordia age, and the weighted average $^{207}Pb/^{206}Pb$ age of 960 ± 7 Ma. The other two analyses gave significantly younger ages at 880-910 Ma. The ca. 950 Ma age is taken as the best estimate of the igneous age for this sample.

MESR49a yielded a homogeneous Hf-isotope population of zircons (n=34), with an average of $^{176}Hf/^{177}Hf = 0.282419 \pm 0.000050$, or εHf_i of 7.7 ± 1.8.

Sample MESR109 and 110 both come from the very small Causinknappen nunatak, which consists of tonalite (MESR110) with garnet-bearing mafic enclaves and schlieren (Fig. 2d). Garnet-free mafic material is also present, which has a sharper contact with the host rock and which we interpret to being a (poorly exposed) dyke; this constitutes sample MESR109.

MESR110 contains clear, virtually colourless zircons, typically with prismatic shape, and up to 300 µm in their longest dimension. Aspect ratios are typically 3:1. They show fine oscillatory zoning in CL imaging. Ten crystals were ablated, and gave U contents of 200-800 ppm. Two zircons are discordant and give $^{207}Pb/^{206}Pb$ ages of 940-950 Ma, and may have been affected by partial resetting by the magma that yielded MESR109 (see below). The other eight spots gave a weighted average $^{207}Pb/^{206}Pb$ age of 979 ± 15 Ma (MSWD = 0.06), and intercept ages at 979 +19/-18 and 66 +280/-60 Ma (Fig. 5k).

This sample yielded a very homogeneous Hf isotopic population: 12 grains gave an average initial $^{176}Hf/^{177}Hf$ ratio of 0.282283 ± 0.000034, or εHf_i of 4.2 ± 1.2.

Zircons in MESR109 are rare and small (100µm), and elongated in shape. Small zircons have aspect ratios up to 4:1, but larger ones are generally 2:1. They are typically cloudy brown in colour, and give a very poor CL response. Only nine crystals could be ablated, of which one grain is clearly older ($^{207}Pb/^{206}Pb$ age >2 Ga). Of the seven other grains, only two show less than 15% discordance; the other five show a combination of Pb-loss and common Pb, yielding $^{207}Pb/^{206}Pb$ ages between 950 and 1570 Ma, and $^{206}Pb/^{204}Pb$ ratios as low as 300. The two least discordant grains, with the highest $^{206}Pb/^{204}Pb$ ratios define a two-point isochron with an upper intercept of 927 +37/-22 Ma (Fig. 5k), which is within error of the weighted mean $^{207}Pb/^{206}Pb$ age of 929 ± 14 Ma, which we take as the best estimate of the igneous age. When the older grain is combined with the two analyses of the old crystal in MESR106, a discordia with intercepts at 550 +33/-32 and 2970 +32/-30 Ma (MWSD 2.2) can be constructed (Fig. 5l).

Only 6 grains were suitably large for Hf isotope analysis, and one of them was the inherited grain. The five igneous grains give a scattered distribution (Fig. 6) with an average of $^{176}Hf/^{177}Hf$ of 0.282408 ± 0.000147, or εHf_i of 6.9 ± 5.2. If an age of 2.97 Ga is taken for the inherited grain, its initial Hf isotopic composition is 0.280821 or εHf_i of -2.1.

7. Geochemistry

In order to facilitate the presentation and discussion of the data, three main groups of samples are defined on the basis of their age: one sample, MESR99, with an age of ca. 1015 Ma; the main group of samples with ages between 995-975 Ma; and the younger samples (960-925 Ma). The main group has been subdivided on the basis of their mineralogy (Fig. 4) into (quartz-)gabbros (nine samples), tonalites (fifteen samples), trondhjemites (four samples), and a single granodiorite (MESR97). The younger samples are quartz-monzodiorite MESR49a from Lågkollane, the quartz-gabbro MESR109 from Causinknappen, and the two granodiorites and a gabbro from the SE of Widerøefjellet (MESR105-107). Note that the samples are referred to by their igneous name from now on, although all are strictly speaking metamorphic rocks.

7.1. Major and trace elements

Fig. 7 shows selected Harker variation diagrams of major and trace elements (all analyses can be found in the Electronic Appendix), while Figs. 8 and 9 show normalised rare earth element (REE) and trace element diagrams.

The main age (995-975 Ma) group of samples shows coherent trends that broadly conform to those expected from a consanguineous group of igneous rocks, related to each other by the fractionation of plagioclase and ferromagnesian mineral phases: CaO (as well as Fe_2O_3*, MnO and MgO) decrease, whereas Na_2O and to a lesser extent K_2O increase with increasing SiO_2 content. The tonalite sample from Causinknappen (MESR110) is unusual in its low sodium and high calcium content. Data for TiO_2 are somewhat scattered on the low-SiO_2 side of the diagram, but decrease from tonalite to trondhjemite. For the trace elements, V (as well as Cr, Ni,

Sc and Co) decrease with increasing SiO_2 content, Y and Zr (as well as Rb, Ba and REE) show a scattered increase, while Sr contents remain more or less constant after an initial increase. REE patterns are typically flat to slightly LREE-enriched for the (quartz-)gabbros, while LREE concentrations increase in tonalitic and trondhjemitic samples. Both positive and negative Ce- and Eu-anomalies occur, unrelated to the modal composition of the samples. Two (undated) samples show somewhat aberrant behaviour: quartz-gabbro MESR18 has higher TiO_2, P_2O_5, Y and REE contents than other samples of this group, while granodiorite MESR97 has higher K_2O, Rb and Ba concentrations.

The one sample that gave a marginally older age at ca. 1015 Ma has the highest SiO_2 content, and lies on the extension of the trend for the 995-975 Ma age group for most variation diagrams. Its REE pattern shows MREE depletion and a very pronounced positive Eu-anomaly (Eu/Eu*=3.3), but is not too dissimilar to that of some of the trondhjemitic samples (Fig. 8a).

Of the younger (960-925 Ma) samples, MESR105-107 as well as MESR49a stand out with respect to their high Sr, and for the felsic samples also high K_2O, Rb and Ba concentrations. Additionally MESR49a also has high Zr, Y, Nb, Ga and REE concentrations compared to the 995-975 age group. The qz-gabbro from Causinknappen, MESR109, has very high TiO_2 (and P_2O_5) contents, and is the only sample to show LREE depletion.

Most samples, apart from some of the most felsic ones, are metaluminous (Fig. 10). They classify as calcic in the modified alkali-lime diagram of Frost et al. (2001), apart from MESR49a, which is alkali-calcic and MESR109 which comes up as marginally calc-alkalic.

7.2 Sr and Nd isotopic systems

Only two samples were analysed for Sr and Nd isotope ratios, since a major body of data on these systems was already presented by Kamei et al. (2013) and Owada et al. (2013). Sr isotopic ratios may be affected by metamorphism, and are therefore less reliable than the Nd isotopic values. The initial $^{87}Sr/^{86}Sr$ ratios are around 0.7033 for both MESR106 and MESR43 (Table 2), which is more or less the value for the Bulk Earth at that time. The $^{143}Nd/^{144}Nd$ ratios are, however, decidedly superchondritic (initial ε_{Nd} +3 to +4), with a somewhat higher value for MESR106 than for MESR43.

7.3 Zircon trace element data

7.3.1 Zircon trace element data

Trace element analyses were performed on some of the zircons for which Hf data were obtained in order to compare them to the whole rock analyses and assess whether the latter could represent liquid compositions, or that they are influenced by cumulate or alteration processes. Since the analyses were quite homogeneous only average data are shown and discussed.

The chondrite-normalised REE patterns (Fig. 11a) show the features expected for zircon, with very low LREE/HREE ratios and a positive Ce-anomaly. There is slightly less than an order of magnitude variation in the absolute concentration of the REE between the samples, with MESR43 having the lowest, and MESR79 the highest concentrations. Most samples display negative Eu-anomalies, but these are much

reduced for MESR106 and MESR104, which both show positive Eu-anomalies in their whole rock REE pattern too. MESR99, which has a very noticeable positive Eu-anomaly in its whole rock REE pattern, shows a clear negative anomaly in its zircon REE pattern.

When the zircon REE-patterns are normalised over the whole rock patterns (Fig. 11b), the results can be interpreted to represent the zircon/liquid distribution coefficient (Kd), provided the whole rock compositions represent liquid compositions. All samples have a steeply sloping Kd pattern, with positive Ce- and negative Eu-anomalies, as is expected from zircon's crystal structure (Belousova et al., 2002). MESR99 displays the strongest Eu-anomaly in its Kd pattern, being as low as 0.04.This lies outside the range found experimentally for varying conditions of temperature and oxygen fugacity (Trail et al., 2012), and outside the trend seen for the other samples (Fig. 11b inset). The positive Eu-anomaly of the whole rock pattern for MESR99 is therefore highly likely to be an accumulative feature. The whole rock patterns for MESR106 and MESR104, with their positive Eu-anomaly, might be a reflection on the liquid composition, since their Kd Eu-anomaly is 0.4, and thereby higher than for the samples without a WR positive Eu-anomaly, and within the experimentally determined range.

Sample MESR43 displays a, potentially metamorphism- or alteration-related, negative Ce-anomaly in its WR REE pattern. The value for the Ce-anomaly in the zircon/WR REE pattern is 5.7, and thereby lower than those for MESR99 or 79, and within the range of experimentally determined values. The question whether this WR Ce-anomaly is a primary feature can therefore not be answered unambiguously, but we think it is related to metamorphism and/or alteration.

Apart from REE, the zircons analysed also contain quantifiable amounts of Th and Nb. High Th/Nb ratios are a feature of subduction-related magmas, and the WR analyses show quite a range of Th/Nb ratios (Fig. 9). Zircon Th/Nb ratios also vary strongly, with a more systematic variation of Nb than Th on a per-sample basis (Fig. 12). There is a broad correlation between Nb contents of the zircons and of the whole rock, in that the sample with the highest WR Nb contents (MESR49a) also has the higher zircon Nb concentrations and lower Th/Nb ratios than, for instance MESR104 with low Nb concentrations and high Th/Nb ratios for both zircon and whole rock. The exception is again MESR99, which has very high WR Th/Nb ratios, and the lowest Nb concentrations, whereas the zircon data are similar to those for MESR79. Calculated zircon/WR ratios for MESR99 are 43 for Nb and 1290 for Th, whereas literature values are 0.3-27 and 11-69 respectively (Nardi et al., 2013). So this confirms the non-liquid composition of the WR sample, as already deduced from the REE patterns. The Nb zircon data for the other samples appears to be compatible with a cogenetic crystal-liquid relationship between zircon and whole rock, since calculated zircon/WR ratios for Nb are 0.5-4.4, while the results for Th are less convincing, with an apparent average Kd of 27-630.

8. Discussion

8.1. U-Pb zircon age groups

Our U-Pb zircon dating shows that the majority of samples have an igneous crystallisation age between 975 and 995 Ma, independent of the analytical technique used for dating (SHRIMP or LA-MC-ICPMS); these ages are similar to, but slightly

younger than those reported by Kamei et al. (2013) and Owada et al. (2013) for the main group of (tholeiitic / low-Ti) meta-igneous rocks (998-995 Ma).

Our three younger ages of 957 ± 8, 947 ± 8 and 929 ± 14 Ma are similar to up to marginally higher than the SHRIMP dates reported previously. Shiraishi et al. (2008) obtained an igneous age of 920 ± 8 Ma for a metatonalite sample from Mefjell, and this age could correspond to the one obtained for our more mafic sample MESR109. Kamei et al. (2013) dated three (CA, high-Sr) samples at 945-930 Ma, while Owada et al. (2013) obtained a single zircon from a high-Ti mafic dyke with an age of 945 ± 9 Ma. An igneous age of 951 ± 17 Ma, so within the time frame of our analyses, has been reported by Shiraishi et al. (2008) for an enderbitic gneiss from northern Brattnipene; this is located north of the Main Shear Zone, but still south of the Main Tectonic Boundary (Fig. 1), and is thus part of the SW terrane. The slightly older ages from sample MESR106 at 1070-1060 Ma are likely to represent inherited zircons. A similar age of 1048 ± 12 Ma was reported by Osanai et al. (2013) for garnet-biotite gneiss from Mefjell South, within the SW-terrane. The ca. 3 Ga single zircons in MESR106 and MESR109 are quite remarkable. Although laboratory cross-contamination can never be completely excluded, no rocks of a similar age were treated in the laboratory at the same time. Also, old ages are not completely unknown from the Sør Rondane Mountains, but only north of the Main Tectonic boundary: Shiraishi et al. (2008) reports a single ca. 3260 Ma grain within a paragneiss from northern Austkampane while Pasteels and Michot (1968) report zircon fractions from granitoids to the SW of Austkampane that yielded an ca. 2700 Ma upper intercept. Within the broader Antarctic context, igneous activity around 2990 Ma has been reported in the Napier Craton (Kelley and Harley, 2005) and similar ages also exist in the Ruker Complex (see overview in Liu et al., 2013).

Whether it is statistically relevant that we only found Archaean zircons in the younger intrusions is unclear.

One of our samples, MESR99, yielded an older age of 1015 ± 4 Ma. Four zircons from a nearby sample, 12B4, give a similar upper intercept age. Similar, inherited U-Pb zircon ages of 1014 ± 15 and 1009 ± 13 Ma have been reported by Shiraishi et al. (2008) from gneiss samples in the NE terrane (Perlebandet and Utnibba), while Osanai et al. (2013) report inherited ages of 1030-1040 Ma from Bamseungen within the meta-igneous sector of the SW terrane.

The ages presented here strengthen the connection between the SW- and NE-terrane of Sør Rondane. The two areas show different P-T-t paths related to the amalgamation of Gondwana, and were also thought to differ in the maximum age of inherited zircon, with ages older than 1100 Ma previously unreported for the SW terrane (Osanai et al., 2013). If we accept the validity of the two ca. 3 Ga inherited zircons presented here, then this distinction has ceased to exist. However, 900-1000 Ma ages are noticeably scarcer in the NE- than the SW-terrane (Shirashi et al., 2008; Osanai et al., 2013), which could be related to the difference in crustal level between the two terranes, as the NE-terrane is dominated by metasedimentary rocks.

Our ages, together with those published previously, reinforce the idea that Meso-Neoproterozoic magmatism in the Sør Rondane Mountains occurred significantly later than in Central and Western Dronning Maud Land where it has been dated at 1130-1060 Ma (Jacobs et al., 2003; 1998), similar to ages found in the South African Natal Belt (McCourt et al., 2006). The area furthest west from Sør Rondane in Antarctica where 900-1000 Ma (Sm-Nd isochron) ages are found is the Schirmacher Hills (Rao et al., 2000; Ravikant, 2006), although these are interpreted to reflect

metamorphism, rather than a magmatic event. Towards the east, there is a scarcity of data for the Yamato-Belgica complex, but Shiraishi et al. (1994) present a U-Pb zircon protolith age of ca. 1000 Ma. From the Lützow-Holm to the Rayner Complex ca.1000 Ma ages are quite common (Shiraishi et al., 2008; Liu et al., 2013), e.g. in the Cape Hinode metatrondhjemites (1017±13 Ma, Shiraishi et al., 2008) and Mawson Coast charnockites (Halpin et al., 2012). This is most widely interpreted as reflecting a connection between this part of Antarctica and Sri Lanka – India – Madagascar prior to Gondwana amalgamation (e.g. Boger et al., 2014). In this reconstruction, the Vijayan Complex of Sri Lanka would be closest to Sør Rondane, and ages of 900-1100 Ma are indeed found there (Kröner et al., 2013).

8.2 Comparative geochemistry

In the following section we compare our data to those published by others to interpret the likely tectonic setting in which the magmas were generated and their similarity to similarly-aged (meta-)igneous rocks within Sør Rondane, neighbouring areas in Antarctica (central Dronning Maud Land and Schirmacher Hills; Mikhalsky and Jacobs, 2004; Rao et al., 2000; Ravikant, 2006) and the Vijayan Complex in Sri Lanka (Milisenda et al., 1994; Kröner et al., 2013). Connections between the Sør Rondane Mountains, the Namuno block of Mozambique and the Central Highlands Complex of Sri Lanka have been proposed by Grantham et al. (2008), based on the available geochronological and structural data. The SHRIMP U-Pb zircon ages for a charnockite from the Ocua and a tonalitic gneiss from the Marupa complex in Mozambique of 994 ± 61 and 951± 44 Ma respectively (Grantham et al., 2008) are indeed similar to the ages reported here, but no geochemical data is available to further investigate the connection.

8.2.1 Relationships within SW-terrane Sør Rondane: tectonic interpretation.

The one sample (MESR99) that gave the older, ca. 1015 Ma, age is more SiO_2-rich than any of the other samples. The homogeneity of the age and Hf isotopic composition of the zircons composition demonstrates that it is an igneous rock. However, its whole rock composition is unlikely to represent a liquid composition, as indicated by the zircon/whole rock trace element ratios, which do not fall within the range for published distribution coefficients. The sample is very rich in quartz and plagioclase (partially replaced by epidote), and has unusually high zirconium and hafnium concentrations compared to its REE contents; we therefore interpret it to be a felsic cumulate or crystal-rich tuff. Considering the similarity in zircon Hf isotope ratios and trace element contents to some of the 995-975 Ma samples, its parental magma must have shown a strong geochemical resemblance to the magmas of this age group, and we will therefore consider it together with these samples. Because of its aberrant whole rock composition and unknown age, qz-gabbro MESR18 may not belong this group. Although the ca. 980 Ma age of Causinknappen tonalite MESR110 falls into the 995-975 Ma age group, its geochemical (low sodium, high calcium) and isotopic characteristics (lower Hf isotopic composition) are aberrant; this could be related to its position further south than the other samples. It lies close to an inferred shear zone (Fig. 1a), and the boundary with the SE Dronning Maud Land Province of Mieth et al. (2014).

Our samples that are interpreted to belong to the main 995 - 975 Ma age group have low TiO_2 (<0.6 wt.%), Sr (<200 ppm) and Zr (<200 ppm) concentrations. They have flat to slightly LREE-enriched rare earth element patterns (at CI-normalised values between 40 and 4), and their zircons show an average εHf of 6.3-7.3. They closely

resemble the 'main lithotype' (tholeiitic biotite-hornblende metatonalite and associated enclaves) of Kamei et al. (2013) and the low-Ti microgabbros of Owada et al. (2013) in terms of Sr/Y, La/Lu, Ga/Al, V/Ti ratios and initial epsilon Nd ratios (Fig. 13), but also the ca. 950 Ma enderbitic gneisses from the Brattnipene area, north of the Main Shear Zone (Shiraishi and Kagami, 1992).

In common with Kamei et al. (2013) and Owada et al. (2013), we interpret the samples from this age group to have formed in an oceanic arc environment. All the hallmarks for a subduction setting are present in the normalised trace element diagrams: negative Nb anomalies, positive Sr anomalies in the gabbros and enrichment in REE relative to the Zr and Hf. The interpretation of an oceanic rather than continental arc is based on the flat REE patterns for the gabbros and the low absolute concentrations of incompatible trace elements. In this respect, our samples resemble data for e.g. the mid-crustal section of the Jurassic Talkeetna oceanic arc (Greene et al., 2006). There is a strong chemical coherence between the mafic, intermediate and felsic samples which is interpreted as a cogenetic relationship. The dominance of intermediate samples (tonalites) is typical for arc terranes (e.g. Reubi and Blundy, 2009). The occurrence of the (quartz-)gabbros as enclaves within the more felsic intrusives, and the crenulated margins on these enclaves (Fig. 2c), implies that both were (partially) liquid at the same time, and it is therefore likely that the intermediate to felsic magmas were derived from the more mafic magmas by crystal fractionation. The presence of a small positive Eu-anomaly in some samples, of which the zircon trace element data show that it is likely to be a feature of the magmatic liquid could be related to the fractionation sequence being dominated by amphibole rather than plagioclase; this is in line with the concave REE patterns for the felsic samples, and the fairly constant Sr concentrations with increasing SiO_2

content. In the less fractionated (quartz-)gabbro samples, it could be a result from preferential mobilisation of divalent Eu during dehydration of the slab in the sub-arc mantle (Bau and Knittel, 1993).

Our samples that have been dated as at 960-925 Ma have variable geochemical characteristics and do not form a coherent group. They are enriched in Sr compared to the older group (leading to higher Sr/Y ratios), and can have high TiO_2 and P_2O_5 contents (MESR109) or high Zr concentrations (MESR49a). REE patterns vary from LREE depleted (MESR109) to LREE-enriched (MESR107). The Nd and Hf isotopic characteristics are marginally more depleted (i.e. higher values) than for the older age group. These characteristics indicate that high-Sr samples MESR105-107 are most closely related to the 920-950 Ma calc-alkaline group of Kamei et al. (2013), while high-Ti sample MESR109 resembles the ca. 950 Ma high-Ti dykes of Owada et al. (2013). Sample MESR49a has uniquely high Nb and Zr concentrations, but could potentially be related to the high-Ti clan of rocks by fractionation processes.

Considering the geochemical variety of magmas present between 960-925 Ma, the interpretation of the tectonic setting is more difficult. Kamei et al. (2013) interpreted their calc-alkaline series as adakites, based on the Sr/Y ratios, reflecting slab melting; Owada et al. (2013) suggested a back-arc environment based on the V versus Ti diagram for his high-Ti dykes. The evidence for an adakitic signature in the felsic samples of this time period is not as strong as for the Cape Hinode metatrondhjemites (Ikeda et al., 1997), which have a much higher La/Lu and Sr/Y ratios (Fig. 13a,b), but a geochemical shift is nevertheless noticeable, also towards slightly more depleted isotopic characteristics. The high-Ti samples are characterised by LREE-depleted patterns and low La/Nb ratios (Fig. 13e), a-typical for arc-related magmatism, and also have Ti-V characteristics more typical for Mid-

Ocean Ridge (MORB) or Back-Arc Basin Basalt (BABB) than for arc-related magmas (Fig. 13d). However, samples with HFSE enrichments compared to 'classical' arc rocks are found both in back-arc basins (Sinton et al., 2003; Sorbadere et al., 2013) and arc settings (Gazel et al., 2011; Kratzmann et al., 2010; Kuritani, 2001; Peate et al., 1997; Sorbadere et al., 2013). In both environments, the geochemical signature can be explained by a small contribution from the subducted slab and a more important role for adiabatic melting of asthenospheric mantle compared to typical arc settings, where melting is mainly induced by a hydrous flux from the slab. Since the degree of melting is smaller than for flux-melting, or for the more extensive adiabatic upwelling at Mid-Ocean Ridges, fluid-immobile incompatible trace elements are more enriched than in either arc or MOR magmas. In an arc setting, this type of high-HFSE magma is typically found when there are heterogeneities within the subducting slab, such as a ridge (Kratzmann et al., 2010; Peate et al., 1997), a seamount chain (Peate et al., 1997) or a hotspot track (Gazel et al., 2011), which can lead to slab tear or break-off, and enhanced mantle upwelling compared to a classical subduction situation. This is also an environment in which adakites can form (Yogodzinski et al., 2001).

The fact that this diverse group of magmas intruded after the typical arc-type magmas at 995-975 Ma indicates that a profound change in tectonic regime has occurred. This is most likely the end of a real subduction scenario, either due to collision with a microcontinent or oceanic plateau, or slab break-off. A limited number of samples with similar geochemical characteristics to the 960-925 Ma adakite-like materials was dated at ca. 770 Ma by Kamei et al. (2013). Whether this reflects resumption of subduction or reworking of pre-existing crust is not clear; the isotopic data permit either interpretation.

8.2.2 Relationships within wider Antarctica and Gondwana

Comparing the geochemistry of 900-1200 Ma samples from different areas in Antarctica, and the Vijayan Complex of Sri Lanka, to those from the SW-terrane of Sør Rondane, there a some clear differences and similarities.

The biotite- and pyroxene-bearing gneisses from the NE-terrane analysed by Grew et al. (1992) for Nd isotopes, and the one gneiss sample from the Yamato Mountains (Shiraishi et al., 2008) extend to marginally lower initial ratios (Fig. 13f); however, major and trace element characteristics were not given, apart from Sm and Nd concentrations, which are similar to the 960-925 Ma samples from the SW-terrane.

The mafic and felsic samples from Cape Hinode (Ikeda et al., 1997; Suda et al., 2008) are very similar in terms of Nd isotopes to the meta-igneous samples from the SW-terrane. The felsic samples are slightly more typically trondhjemitic in trace element composition, as described before. The mafic samples are similar to the (quartz-)gabbros.

The orthogneisses from Central Dronning Maud Land (Jacobs et al, 1998; Mikhalsky and Jacobs, 2004) overlap with, but extend to lower values for initial Nd isotopic ratios, similar to the gneisses from the NE-terrane. However, they are geochemically very different, and have much higher contents of (relatively immobile) incompatible elements, such as the REE, Zr, Th and Nb (Fig. 13a, c, e). Similarly, the granulites from Schirmacher Hills show a clear overlap in Nd isotopes (Rao et al., 20000; Ravikant, 2006), but Ti, Nb and Zr contents are significantly enriched. The granitoid gneisses of the Vijayan Complex (Sri Lanka) largely overlap with the gneisses from Central Dronning Maud Land, rather than with our Sør Rondane samples, in geochemistry and isotopic composition. The Hf isotopic composition of the Vijayan

zircons is also typically lower than that of the Sør Rondane samples (Fig. 14a). Although our sample MESR49a shows similarly enriched trace element characteristics to CDML, Schimacher and Vijayan, it distinguishes itself with its depleted Hf isotopic signature for the zircons (Fig. 14a)

So the meta-igneous sector of the SW-terrane compares poorly to the Central Dronning Maud Land orthogneisses in both age (younger) and geochemical composition (more depleted). Despite the overlapping ages and Nd isotopic composition, the samples from Schirmacher Hills do not match in geochemical composition, while the Vijayan complex is both marginally older (up to 1100 Ma), and more enriched in Nd and Hf isotopic signature as well as trace element composition. A reasonably good match exists with the mafics and metatrondhjemites from Cape Hinode, although the latter are ca. 1015 Ma rather than <960 Ma for the Sør Rondane samples that most closely match them in geochemical composition. Not only this age difference is problematic in proposing a match between the two areas, but also the fact that samples from the Lützow-Holm Complex that lie geographically between Cape Hinode and Sør Rondane have Nd isotopic compositions that point towards a more significant role for crustal reworking (Shiraishi et al., 2008; Fig. 14b) – and the presence of the Main Tectonic Boundary, which separates the SW- and NE-terranes. Rocks from the Rayner Complex (fig. 1a), where ca. 900-1000 Ma ages are common too (Boger et al., 2000; Corvino et al., 2008; Mikhalsky and Sheraton, 2011; Grew et al., 2012; Halpin et al., 2012), extend to even more isotopically enriched values (Fig. 14b), reflecting a much longer crustal prehistory.

8.3 Timeline of events and possible tectonic scenarios

The data and comparison shown here have implications for both the Rodinia and Gondwana supercontinents. The disparity in igneous ages between Central Dronning Maud Land and Sør Rondane clearly shows that the latter was more closely related to the Indo-Antarctic Craton (Sri Lanka – India – Madagascar) whereas the former shows strong ties with the Kalahari Craton, being a close match to the South African Natal Belt.

Our data confirms that the meta-igneous sector of the SW-terrane was formed in an oceanic arc setting around 995-975 Ma, and we interpret the signature of the younger rocks to reflect stalling subduction from 950 Ma onwards. No deformation or metamorphism has been recognised in the area around this time, so the halting of the subduction process may be a far-field effect of a collision elsewhere. The dimensions of the meta-igneous sector of the tonalite terrane are more in keeping with either N- or S-dipping subduction in present-day coordinates (rather than E or W), but we have no constraints on the vergence. The rare occurrence of Archaean inherited zircons within the <960 Ma intrusives suggests the proximity to an older craton, which may have been the collider that halted subduction. This could have been part of the aeromagnetically defined Southeast-Dronning Maud Land (SE-DML) Province of Mieth et al. (2014), located directly southwest of the meta-igneous sector. However, it could also be the craton from which the sediments, which are now found in the NE-terrane, have been shed, in which case a more easterly location seems more plausible – although it is unclear what the relative positions of the SW- and NE-terranes were at this stage.

The northern, dominantly supracrustal, sector of the SW-terrane seems related to the meta-igneous terrane in terms of ages and geochemical composition, even

though the two sectors are separated by the much younger dextral Main Shear Zone of Pan-African age (Ruppel, 2012).

The ca. 770 Ma ages for calc-alkaline magmatism in the SW-terrane reported by Kamei et al. (2013) can be interpreted to reflect resumption of subduction. This age and type of magmatism is also known from Sri Lanka (Wanni Complex, Willbold et al., 2004) and Madagascar (see overview by Boger et al., 2014, in press). However, Central and Western Dronning Maud Land were part of Rodinia (Powell and Pisarevsky, 2002), which was in the process of splitting up around this time, and do not appear to record this phase of magmatism. Zircons with 800-700 Ma ages are also found in Schirmacher Hills (Mikhalsky et al., 2011) and within a metadiorite in the NE-terrane of Sør Rondane (Osanai et al., 2013).

The next event is the 650-600 Ma high-grade metamorphism in Sør Rondane (see overview of geochronology in Osanai et al., 2013), which has also been recognised in the Yamato Mountains (Asami et al., 2005) as well as Schirmacher Hills (Ravikant et al., 2004), but not in the Lützow-Holm area (Asami et al., 2005, Shiraishi et al., 2008). This may point towards a crustal boundary between the Yamato Mountains and Lützow-Holm area, as also proposed on the basis of magnetic anomalies (Osanai et al., 2013). For Sør Rondane, the ca. 600 Ma metamorphic event has been linked to the collision between the SW- and NE-terrane, as the downgoing and overthrust blocks respectively. The Dufekfjellet granite (Li et al., 2006; Fig. 1) intruded at the same time (ca. 620 Ma) into the SW-terrane, so into the low-grade portion of the downgoing block, which seems somewhat mysterious from a tectonic point of view, unless another block was being underthrust underneath the SW-terrane from the south. This could then be the SE-DML Province.

The final event is wide-spread intrusion of granitoids and minor syenites (570-510 Ma) in both the SW- and NE-terrane, which were amalgamated at this stage, and associated retrograde metamorphism.

On a larger scale, the juxtaposition of terranes with both ca. 630 and ca. 550 Ma metamorphic ages has also been noted by Boger et al. (in press) for the Vohibory-Androyen and Anosyen domains of SW Madagascar, has been and connected to the events in Antarctica and eastern Africa. Collision between the Vohibory and Androyen terrane was interpreted to have occurred around 630 Ma, so at a similar time to the inferred collision between the NE- and SW-terrane in Sør Rondane. It was followed by collision with the Androyen Terrane, connected to greater India, at ca. 550 Ma. Boger et al. (in press) extend this scenario into Antarctica with the Sør Rondane-Yamato domain (containing ca. 630 Ma ages) colliding with the Lützow-Holm area around 550 Ma during the final amalgamation of Gondwana. Although the Madagascan Vohibory Domain resembles the meta-igneous sector of the SW-terrane of Sør Rondane in being a juvenile oceanic arc terrane, the Vohibory protoliths were formed at 850-700 Ma (Jöns and Schenk, 2008), rather than around 980 Ma. Also, the inferred vergence of the ca. 630 Ma collision in Madagascar is opposite to what has been suggested for the SW- and NE-terranes of Sør Rondane, so a simple one-to-one correlation between SW Madagascar and Sør Rondane does not exist. However, it confirms the idea that Sør Rondane holds an important place in the final amalgamation of Gondwana.

Conclusions

- The meta-igneous sector of the SW-terrane of Sør Rondane was the mid-crustal part of a juvenile oceanic arc terrane around 1020-975 Ma, as indicated by whole rock trace element patterns typical for subduction-related magmas (negative Nb anomalies in mantle-normalised diagrams, positive LREE/HFSE ratios), combined with a high (typically ca. +7) zircon initial epsilon Hf and fairly flat REE patterns. Comparison of zircon and whole rock REE patterns suggest that some of the moderately positive Eu-anomalies may be a feature of the magmatic liquid rather than reflecting cumulate processes.

- Younger igneous samples (960-920 Ma) are more variable: they are either characterised by high Sr/Y rations ('adakitic' signature) or have a reduced to absent subduction signature in terms of trace element patterns; all have higher zircon Hf isotopic ratios. This is interpreted as signifying the end of subduction, and magmatism related to adiabatic upwelling of subduction-modified or unadulterated depleted mantle, and/or slab melting.

- Rare inherited zircons with Archaean and late Mesoproterozoic ages in the <960 Ma intrusives could indicate increasing proximity to a cratonic area, potentially the fragment that caused subduction to halt.

- Compared to neighbouring areas in Antarctica and in a wider Gondwanan context, the meta-igneous sector of the SW-terrane is unique with respect to the combination of protolith age, geochemical and isotopic signature.

- The 1000-900 Ma ages are younger than those of the classic 'Grenville' orogeny (as seen in central and western Dronning Maud Land and the South African Natal Belt) that formed Rodinia, and more similar to ages observed in India - Sri Lanka – Madagascar. This supports the idea that greater India was not part of or was located

in a peripheral position to the Rodinian supercontinent (Powell and Pisarevsky, 2002).

- The ca. 630 and 550 Ma metamorphic and igneous history of Sør Rondane documented by other workers reflects the progressive amalgamation of Gondwana, and may be connected to events in SW Madagascar and eastern Africa (Boger et al., in press).

Acknowledgements:

The whole GEA II team would like to thank the helicopter pilots Knut Wagner, Florian Tauber and Jörn Hergenröder of Sky Heli, Germany, for their flying skills, and Alain Hubert, Gigi Johnson-Amin and the whole crew of the Belgian 'Princess Elisabeth' Station for their hospitality and support during the field season. The analytical work was funded by a grant from the South African National Research Foundation to MAE; Carishma Ramchurran and Pat Suthan are thanked for their help with the analytical work at UKZN, and Christel Tinguely, Phil Janney and Petrus Le Roux at UKZN. J. Jacobs, N. Lucka and M. Elburg are indebted to BGR for the invitation to participate at the GEA expeditions. J. Jacobs wishes to thank Alfred-Wegener-Institute for Polar and Marine Research (AWI) and M. Elburg International Polar Foundation (IPF) and BELARE for providing polar clothing. The study was partly supported by the Deutsche Forschungsgemeinschaft (Grants LA 1080/9 to A. Läufer, BGR, and LI 745/15 to F. Lisker, Univ. Bremen) in the framework of the priority programme “Antarctic Research with comparative investigations in Arctic ice areas”. J. Jacobs work was funded in part by NFR-NARE.The manuscript benefitted greatly from reviews by A. Kamei and presumably S. Boger; their considerable efforts have been very much appreciated.

Figure captions

Fig. 1: a: Regional tectonic framework of the Sør Rondane Mountains, eastern Dronning Maud Land. Sør Rondane is located halfway between the Grunehogna and the Napier Cratons. The Grunehogna Craton is surrounded by the Mesoproterozoic Maud Belt with African (Kalahari) affinities, whilst the Napier Craton, which is fringed by the ca. 1.4-0.9 Ga Rayner Complex, has affinities to greater India. The Forster Magnetic Anomaly (FMA) has been recognised as a significant Late Neoproterozic suture zone. The area may be dissected by additional Late Neoproterozoic suture zones that are, however, less well defined.

Abbreviations: B – Belgica Mts., BT – Beaver Terrane, CDML – central Dronning Maud Land, EAAO – East African-Antarctic Orogen, FT – Fischer Terrane, LC – Lambert Complex, LHC – Lützow-Holm Complex, MC – Mawson coast, MRL – Mac.Robertson Land, NPCM – northern Prince Charles Mts., PB – Prydz Bay, SH – Schirmacher Hills, WDML – western Dronning Maud Land, Y – Yamato Mts., ØC – Øygarden Complex.

B: Geological map of the Sør Rondane mountains after Kamei et al. (2013), Osanai et al. (2013), Shiraishi et al. (1997) and our own data, indicating the location of the samples analysed in this study.

Fig. 2: Field photographs of the sampled lithologies. A: Metatonalite with quartz-gabbroic enclave on central Widerøefjellet (sample MESR38). B: Outcrop at the east

side of Widerøefjellet. Sample MESR99 was taken from the most leucocratic material. Inset shows person for scale. C: Enclave-bearing metatonalite on the east side of Niels Larsenfjellet (MESR101-102). Note the scalloped rims of the mafic enclaves, indicative of an origin by magma mingling. D: Causinknappen nunatak, showing intermingling of mafic and felsic (MESR110) material, and the presence of garnet. E: Undeformed enclave-bearing metatonalite from which sample 07C1 was taken. F: Area from which sample 07A1 originates, interpreted to be the deformed equivalent of panel E.

Fig. 3: Photomicrographs of selected samples. A: Sample MESR97, with quartz phenocrysts in a fine-grained matrix, interpreted to represent a shallow-intrusive origin of the sample. B: Sample MESR100, showing broad oscillatory zoning in the plagioclase crystal, interpreted to be a relict of the igneous protolith. C: Sample MESR99, the oldest sample analysed, consisting predominantly of quartz and plagioclase, partially altered to epidote. This sample could either be a felsic cumulate, or a crystal-rich tuff; the texture is clearly metamorphic, and does not permit a choice between the two options. D: Sample MESR104, containing subhedral garnet, interpreted to be of metamorphic origin.

Fig. 4: Relevant parts of QAPF (Le Maitre, 2002) and Ab-An-Or normative diagrams (Barker, 1979) on which the classification of the samples has been based.

Fig. 5: Zircon U-Pb data. Only the analytical points that were used for age calculation are shown; full analyses are given in the Electronic Appendix. All uncertainties are 2 σ. A-D: Sample analysed by SHRIMP (Curtin University, W. Australia); E-L: samples

analysed by LA-MC-ICPMS (Oslo University, Norway), which were also analysed for Lu-Hf and trace elements. Zircon portraits are BSE images, apart for panels G, H, K and L (CL). The c. 3 Ga zircon in sample MESR106 (panel L) was only imaged after ablation, hence the crater.

Fig. 6. Box-and-whisker plot of initial zircon Hf isotopic composition versus age, with labelled contour lines for epsilon Hf. Because of the limited number of zircons analysed for MESR109, only the data points are shown. Other data points shown are outliers from the main population. The reference line with $^{176}Lu/^{177}Hf$ = 0.015 indicates the typical evolution of crust with a depleted mantle extraction age of ca. 1.4 Ga, which passes through most of the ca. 995-975 samples.

Fig. 7: Harker variation diagrams for selected oxides and elements. Legend is given in the figure.

Fig. 8: CI-normalised Rare Earth Element diagrams. Normalising values from Evensen et al. (1978). Dated samples given in bold lines. A: Patterns for the 995-975 Ma trondhjemites, granodiorite and the one older, high-SiO_2 tonalite MESR99. B: Patterns for the 995-975 Ma tonalites. C: Gabbroic samples assumed to belong to the 995-975 Ma age group. D: Mafic and felsic samples 960-925 Ma.

Fig. 9: Primitive mantle-normalised trace element patterns. Normalising values from Palme and O'Neill (2003). Legend and panels as for Fig. 8.

Fig. 10: Classification diagrams. A: Aluminium-saturation index (ASI = molar $Al_2O_3/(Na_2O+K_2O+Na_2O)$ versus SiO_2. B: Modified alkali-lime diagram (Frost et al., 2001). Most data classifies as being calcic, with MESR49a being a notable exception.

Fig. 11: Zircon trace element data, averaged per sample. A: Chondrite-normalised REE patterns for average zircons from the different sample, showing the positive Ce- and negative Eu-anomalies expected from the zircon's crystal chemistry. Samples MESR104 and 106 display a reduced negative Eu-anomaly compared to the other samples. B: Whole rock-normalised zircon REE patterns. The very low zircon/whole rock Eu ratio for MESR99 indicates that the whole rock composition is unlikely to represent a liquid. Samples MESR104 and 106 have a Eu-anomaly within the range expected for zircon/liquid distribution coefficients, indicating that the positive Eu-anomaly in the whole rock samples is unlikely to be a cumulate effect.

Fig. 12: Nb versus Th concentrations for zircons. Note log scale on both axes. Although not highly systematic, there is a relationship between whole rock and zircon data, with sample MESR104 also showing a pronounced negative Nb anomaly for the whole rock, whereas this anomaly is very much reduced for MESR49a.

Fig. 13: Comparison between samples analysed in the present study and published data; symbols as in Fig. 7 and given in diagram. Panels on left show data from the SW-terrane of Sør Rondane: ca. 995 Ma tholeiites, 920-945 and ca. 770 Ma calc-alkaline: Kamei et al. (2013); low-Ti enclaves (ca. 995) and high-Ti dykes (ca. 920): Owada et al. (2013); ca. 950 Ma enderbites: Shiraishi and Kagami (1992). Panels on

right show data from the broader region: Central Dronning Maud Land: Jacobs et al. (1998), Mikhalsky and Jacobs (2004); Cape Hinode trondhjemite: Ikeda et al. (1997); Cape Hinode mafics: Suda et al. (2008); Schirmacher Hills: Rao et al. (2000); Ravikant (2008); Vijayan Complex, Sri Lanka: Milisenda et al. (1994), Kröner et al. (2013. A: Sr/Y vs. Y (note log scale for y-axis); B: La/Lu (log scale) vs SiO_2; C: Zr versus 10000*Ga/Al with fields for different granite types from Whalen et al. (1987); D: V versus Ti/1000 with fields for different types of basalts from Shervais (1982); E: Nb versus La (double log scale); F: initial εNd value versus $^{147}Sm/^{144}Nd$, with additional data from Shiraishi et al. (2008) for Yamato Mts, and Grew et al. (1992) for NE-terrane gneisses.

Fig. 14. A: As Fig. 6, but with data for the Vijayan Complex of Sri Lanka (SL sample numbers) from Kröner et al. (2013). B: Present-day $^{143}Nd/^{144}Nd$ versus $^{147}Sm/^{144}Nd$; data sources and symbols as for Fig. 13, with additional data from the compilation by Shiraishi et al. (2008). Reference line for εNd=0 at 1000 Ma shown for comparison. Data for the Lützow-Holm and Rayner Complex extend to far lower $^{143}Nd/^{144}Nd$ ratios than the Sør Rondane samples, indicative of an old crustal component in their source.

Table 1: Summary of zircon U-Pb ages and Hf isotopes

Table 2: Representative whole rock analyses.

References:

Asami, M., Suzuki, K., Grew, E.S., 2005. Monazite and zircon dating by the chemical Th-U-total Pb isochron method (CHIME) from Alasheyev Bight to Sør Rondane Mountains, East Antarctica: a reconaissance study of the Mozambique Suture in Eastern Queen Maud Land. Journal of Geology 113, 59-82.

Barker, F., 1979. Trondhjemite: definition, environment and hypotheses of origin. In: Barker, F. (Ed.), Trondhjemites, Dacites, and Related Rocks. Elsevier Scientific Publishing, Amsterdam pp. 1-12.

Bau, M., Knittel, U., 1993. Significance of slab-derived partial melts and aqueous fluids for the genesis of tholeiitic and calc-alkaline island-arc basalts - evidence from Mt Arayat, Philippines. Chemical Geology 105, 233-251.

Belousova, E. A., Griffin, W. L., O'Reilly, S. Y., Fisher, N. I., 2002. Igneous zircon: trace element composition as an indicator of source rock type. Contributions to Mineralogy and Petrology 143, 602-622.

Boger, S. D., 2011. Antarctica - Before and after Gondwana. Gondwana Research 19, 335-371.

Boger, S. D., Hirdes, W., Ferreira, C.A.M., Schulte, B., Jenett, T., Fanning, C.M., 2014. From passive margin to volcano–sedimentary forearc: The Tonian to Cryogenian evolution of the Anosyen Domain of southeastern Madagascar. Precambrian Research 247, 159-186.

Boger, S. D., Carson, C. J., Wilson, C. J. L., Fanning, C. M., 2000. Neoproterozoic deformation in the Radok Lake region of the northern Prince Charles Mountains, east Antarctica; evidence for a single protracted orogenic event. Precambrian Research 104, 1-24.

Boger, S. D., Hirdes, W., Ferreira, C. A. M., Jenett, T., Dallwig, R., Fanning, C. M., in press. The 580–520 Ma Gondwana suture of Madagascar and its continuation into Antarctica and Africa. Gondwana Research, doi: 10.1016/j.gr.2014.08.017

Corvino, A. F., Boger, S. D., Henjes-Kunst, F., Wilson, C. J. L., Fitzsimons, I. C. W., 2008. Superimposed tectonic events at 2450 Ma, 2100 Ma, 900 Ma and 500 Ma in the North Mawson Escarpment, Antarctic Prince Charles Mountains. Precambrian Research 167, 281-302.

Elburg, M. A., Andersen, T., Bons, P. D., Simonsen, S. L., Weisheit, A., 2013. New constraints on Phanerozoic magmatic and hydrothermal events in the Mt Painter Province, South Australia. Gondwana Research 24, 700-712.

Evensen, N. M., Hamilton, P. J., O'Nions, R. K., 1978. Rare-earth abundances in chondritic meteorites. Geochimica et Cosmochimica Acta 42, 1199-1212.

Frost, B. R., Barnes, C. G., Collins, W. J., Arculus, R. J., Ellis, D. J., Frost, C. D., 2001. A geochemical classification for granitic rocks. Journal of Petrology 42, 2033-2048.

Gazel, E., Hoernle, K., Carr, M. J., Herzberg, C., Saginor, I., van den Bogaard, P., Hauff, F., Feigenson, M., Swisher, C., 2011. Plume–subduction interaction in southern Central America: Mantle upwelling and slab melting. Lithos 121, 117-134.

Grantham, G. H., Macey, P. H., Ingram, B. A., Roberts, M. P., Armstrong, R. A., Hokada, T., Shiraishi, K., Jackson, C., Bisnath, A., Manhica, V., 2008. Terrane correlation between Antarctica, Mozambique and Sri Lanka; comparison of geochronology, lithology, structure and metamorphism and possible implications for the geology of southern Africa and Antarctica, *in*

Satish-Kumar, M., Motoyoshi, Y., Osanai, Y., Hiroi, Y., and Shiraishi, K., eds., Geodynamic Evolution of East Antarctica, Volume 308: London, Geological Society, p. 91-119.

Greene, A.R., DeBari, S.M., Kelement, P.B., Blusztajn, J., Clift, P.D., 2006. A Detailed Geochemical Study of Island Arc Crust: the Talkeetna Arc Section, South–Central Alaska. Journal of Petrology 47, 1051-1093.

Grew, E. S., Carson, C. J., Christy, A. G., Maas, R., Yaxley, G. M., Boger, S. D., and Fanning, C. M., 2012. New constraints from U-Pb, Lu-Hf and Sm-Nd isotopic data on the timing of sedimentation and felsic magmatism in the Larsemann Hills, Prydz Bay, East Antarctica. Precambrian Research 206, 87-108.

Grew, E. S., Manton, W. I., Asami, M., Makimoto, H., 1992. Reconnaissance geochronologic data on Proterozoic polymetamorphic rocks of the eastern Sør Rondane Mountains, East Antarctice, *in* Yoshida, T., Kaminuma, K., and Shiraishi, K., eds., Recent Progress in Antarctic Earth Science: Tokyo, Terra, p. 37-44.

Halpin, J. A., Daczko, N. R., Milan, L. A., Clarke, G. L., 2012. Decoding near-concordant U–Pb zircon ages spanning several hundred million years: recrystallisation, metamictisation or diffusion? Contribution to Mineralogy and Petrology 163, 67-85.

Ikeda, Y., Shiraishi, K., 1998. Petrogenesis of the tonalitic rocks from the Sør Rondane Mountains, East Antarctica. Polar Geosciences 11, 143-153.

Ikeda, Y., Shiraishi, K., Yanai, K., 1997. Petrogenesis of the meta-trondhjemites from Cape Hinode, East Antarctica. Proc. NIPR Symp. Anarct. Geosci. 10, 102-110.

Jacobs, J., Fanning, C. M., Bauer, W., 2003. Timing of Grenville-age vs. Pan-African medium- to high-grade metamorphism in western Dronning Maud Land (East Antarctica) and significance for correlations in Rodinia and Gondwana. Precambrian Research 125, 1-20.

Jacobs, J., Fanning, C. M., Henjes-Kunst, F., Olesch, M., Paech, H. J., 1998. Continuation of the Mozambique Belt into East Antarctica: Grenville-age metamorphism and polyphase Pan-African high-grade events in central Dronning Maud Land. Journal of Geology 106, 385-406.

Jöns, N. and Schenk, V., 2008. Relics of the Mozambique Ocean in the central East African Orogen: evidence from the Vohibory Block of southern Madagascar. Journal of Metamorphic Geology 26, 17-28.

Kamei, A., Horie, K., Owada, M., Yuhara, M., Nakano, N., Osanai, Y., Adachi, T., Hara, Y., Terao, M., Teuchi, S., Shimura, T., Tsukada, K., Hokada, T., Iwata, C., Shiraishi, K., Ishizuka, H., Takahashi, Y., 2013. Late Proterozoic juvenile arc metatonalite and adakitic intrusions in the Sor Rondane Mountains, eastern Dronning Maud Land, Antarctica. Precambrian Research 234, 47-62.

Kelley, N. M., Harley, S. L., 2005. An integrated microtextural and chemical approach to zircon geochronology: refining the Archaean history of the Napier Complex, east Antarctica. Contributions to Mineralogy and Petrology 149, 57-84.

Kratzmann, D., Carey, S., Scasso, R., Naranjo, J.-A., 2010. Role of cryptic amphibole crystallization in magma differentiation at Hudson volcano, Southern Volcanic Zone, Chile. Contributions to Mineralogy and Petrology 159, 237-264.

Kröner, A., Rojas-Agramonte, Y., Kehelpannala, K. V. W., Zack, T., Hegner, E., Geng, H. Y., Wong, J., Barth, M., 2013. Age, Nd–Hf isotopes, and geochemistry of the Vijayan Complex of eastern and southern Sri Lanka: A Grenville-age magmatic arc of unknown derivation. Precambrian Research, 234, 288-321.

Kuritani, T., 2001. Replenishment of a mafic magma in a zoned felsic magma chamber beneath Rishiri Volcano, Japan. Bulletin of Volcanology, 533-548.

Le Maitre, R. W., 2002. Igneous Rocks - A Classification and Glossary of Terms. Cambridge, Cambridge University Press.

Li, Z., Du, Z., Yang, S., Chen, H., Song, B., Liu, D., 2006. First report of zircon SHRIMP U-Pb dating from the Dufek granite in the Sør Rondane Mountains, East Antarctica. Journal of Zhejiang University Science A, 315–319, http://dx.doi.org/10.1631/jzus.2006.AS0315.

Liu, X., Zhao, Y., Hu, J., 2013. The c. 1000-900 Ma and c. 550-500 Ma tectonothermal events in the Prince Charles Mountains-Prydz Bay region, East Antarctica, and their relations to supercontinent evolution: Geological Society, London, Special Publications 383 95-112.

McCourt, S., Armstrong, R.A., Grantham, G.H., Thomas, R.J., 2006. Geology and evolution of the Natal belt, South Africa. Journal of African Earth Sciences 46, 71-92.

Meert, J. G., 2003. A synopsis of events related to the assembly of eastern Gondwana. Tectonophysics 362, 1-40.

Mieth, M., Jacobs, J., Ruppel, A., Damaske, D., Låufer, A., Jokat, W., 2014. New detailed eromagnetic and geological data of eastern Dronning Maud Land:

Implications for refining the tectonic and structural framework of Sør Rondane, East Antarctica. Precambrian Research 245, 174-185.

Mikhalsky, E. V., Jacobs, J., 2004. Orthogneisses in central Dronning Maud Land, East Antarctica: their origin and tectonic setting, *in* Paech, H.-J., ed., International GeoMaud expedition of the BGR to central Dronning Maud Land in 1995/96 – Geological results., Geologisches Jahrbuch, B 96, Schweizerbart science publishers, p. 49–76.

Mikhalsky, E. V., Sheraton, J. W., 2011. The Rayner Tectonic Province of East Antarctica: Compositional Features and Geodynamic Setting. Geotectonics 6, 496-512.

Mikhalsky, E. V., Jacobs, J., Fanning, M., 2011, New U-Pb zircon and Sm-Nd whole-rock data for metamorphic rocks of central Dronning Maud Land: implications for the structural evolution of Neoproterozoic to Cambrian events in Gondwana. 11th Internation Symposium on Antarctic Earth Sciences, Edinburgh 2011, 305

Milisenda, C. C., Liew, T. C., Hofmann, A. W., Kohler, H., 1994. Nd isotopic mapping of the Sri Lanka basement - update, and additional constraints from Sr isotopes. Precambrian Research 66, 95-110.

Nardi, L. V. S., Formoso, M. L. L., Muller, I. F., Fontana, E., Jarvis, K., Lamarao, C., 2013. Zircon/rock partition coefficients of REEs, Y, Th, U, Nb, and Ta in granitic rocks: Uses for provenance and mineral exploration purposes. Chemical Geology 335, 1-7.

Osanai, Y., Nogi, Y., Baba, S., Nakano, N., Adachi, T., Hokada, T., Toyoshima, T., Owada, M., Satish-Kumar, M., Kamei, A., Kitano, I., 2013. Geologic evolution of the Sor Rondane Mountains, East Antarctica: Collision tectonics proposed

based on metamorphic processes and magnetic anomalies. Precambrian Research234, 8-29.

Owada, M., Kamei, A., Horie, K., Shimura, T., Yuhara, M., Tsukada, K., Osanai, Y., Baba, S., 2013. Magmatic history and evolution of continental lithosphere of the Sor Rondane Mountains, eastern Dronning Maud Land, East Antarctica. Precambrian Research 234, 63-84.

Palme, H., O'Neill, H. S. C., 2003. Cosmochemical estimates of mantle composition, *in* Carlson, R. W., Holland, H. D., and Turekian, K. K., eds., Treatise on Geochemistry, vol.2, The Mantle and Core, Volume 2: New York, Elsevier, pp. 1-38.

Pasteels, P., Michot J., 1968. Nouveaux résultats géochronologiques obtenus par la méthode U-Pb sur des zircons des monts Sør-Rondane (Antarctique). Annales de la Société Géologique de Belgique 91, 283-303.

Peate, D. W., Pearce, J. A., Hawkesworth, C. J., Colley, H., Edwards, C. M. H., Hirose, K., 1997. Geochemical variations in Vanuatu Arc Lavas: the role of subducted material and a variable mantle wedge composition. Journal of Petrology 38, 1331-1358.

Powell, C.M., Pisarevsky, S.A., 2002. Late Neoproterozoic assembly of East Gondwana. Geology 30, 3-6.

Rao, D.R., Rashid, S.A., Panthulu, G.V.C., 2000. Origin of Mg-Metatholeiites of the Schirmacher Region, East Antarctica: Constraints from Trace Elements and Nd-Sr Isotopic Systematics. Gondwana Research 3, 91-104.

Ravikant, V., 2006. Sm-Nd Isotopic evidence for Late Mesoproterozoic metamorphic relics in the East African Orogen from the Schirmacher Oasis, East Antarctica. Journal of Geology 114, 615-625.

Ravikant, V., Bhaskar Rao, Y. J., Gopalan, K., 2004. Schirmacher Oasis as an extension of the Neoproeterozoic East African Orogen into Antarctica: new Sm-Nd isochron age constraints. Journal of Geology 112, 607-616.

Ravikant, V., Laux, J. H., Pimentel, M. M., 2007. Sm-Nd and U-Pb isotopic constraints for crustal evolution during Late Neoproterozoic from rocks of the Schirmacher Oasis, East Antarctica: geodynamic development coeval with the East African Orogeny, *in* Cooper, A. K. et al. (Eds.), Antarctica: A keystone in an changing world - Online Proceedings for the Tenth International Symposium on Antarctic Earth Sciences, Volume 2007-1047, USGS Geological Survey, http://pubs.usgs.gov/of/2007/1047.

Reubi, O., Blundy, J., 2009. A dearth of intermediate melts at subduction zone volcanoes and the petrogenesis of arc andesites. Nature 461, 1269-1273.

Ruppel, A. S., 2012. Structural evolution of the Main Shear Zone in Sr Rondane, East Antarctica. MSc thesis, University of Bremen.

Shervais, J. W., 1982. Ti-V plots and the petrogenesis of modern and ophiolitic lavas: Earth and Planetary Science Letters 59, 101-118.

Shiraishi, K., Dunkley, D. J., Hokada, T., Fanning, C. M., Kagami, H., Hamamoto, T., 2008. Geochronological constraints on the Late Proterozoic to Cambrian crustal evolution of eastern Dronning Maud Land, East Antarctica: a synthesis of SHRIMP U–Pb age and Nd model age data, *in* Satish-Kumar, M., Motoyoshi, Y., Osanai, Y., Hiroi, Y., Shiraishi, K. (Eds.), Geodynamic Evolution of East Antarctica: A key to the East-West Gondwana connection, Volume 308: London, The Geological Society of London, p. 21-67.

Shiraishi, K., Ellis, D.J., Hiroi, Y., Fanning, C.M., Motoyoshi, Y., Nakai, Y., 1994. Cambrian orogenic belt in East Antarctica and Sri Lanka: Implications for Gondwana Assembly. Journal of Geology 102, 47-65.

Shiraishi, K., Osanai, Y., Ishizuka, H., Asami, M., 1997. Geological Map of Sør Rondane Mountains. National Institute of Polar Research, scale 1:250,000.

Shiraishi, K., Osanai, Y., Tainosho, Y., Takahashi, K., Tsuchiya, N., Kojima, S., Yanai, K., Moriwaki, K., 1992. Antarctic Geological Map Series, Sheet 32 Widerøefjellet: National Polar Institute, scale 1:100,000.

Sinton, J. M., Ford, L. L., Chappell, B., McCulloch, M. T., 2003. Magma genesis and mantle heterogeneity in the Manus back-arc basin, Papua New Guinea. Journal of Petrology 44, 159-195.

Sorbadere, F., Schiano, P., Métrich, N., Bertagnini, A., 2013. Small-scale coexistence of island-arc- and enriched-MORB-type basalts in the central Vanuatu arc. Contributions to Mineralogy and Petrology 166, 1305-1321.

Suda, Y., Kawano, Y., Yaxley, G., Korenaga, H., Hiroi, Y., 2008, Magmatic evolution and tectonic setting of metabasites from Lützow-Holm Complex, Antarctica, *in* Satish-Kumar, M., Motoyoshi, Y., Osanai, Y., Hiroi, Y., Shiraishi, K. (Eds.), Geodynamic evolution of East Antarctica, Volume 308: London, Geological Society, p. 211-233.

Trail, D., Watson, E. B., Tailby, N. D., 2012. Ce and Eu anomalies in zircon as proxies for the oxidation state of magmas. Geochimica et Cosmochimica Acta 97, 70-87.

Van Autenboer, T., Michot, J., Picciotto, E., 1964. Outline of the geology and petrology of the Sør-Rondane Mountains, Dronning Maud Land, *in* Adie, R. J.,

ed., Antarctic Geology: Amsterdam, North Holland Publishing Company, p. 501-514.

Whalen, J.B., Currie, K.L., Chappell, B.W., 1987. A-type granites: geochemical characteristics, discrimination and petrogenesis. Contributions to Mineralogy and Petrology 95, 407-419.

Willbold, M., Hegner, E., Kleinschrodt, R., Stosch, H. G., Kehelpannala, K. V. W., Dulski, P., 2004. Geochemical evidence for a Neoproterozoic magmatic continental margin in Sri Lanka - relevance for the Rodinia-Gondwana supercontinent cycle. Precambrian Research 130,185-198.

Yogodzinski, G.M., Lees, J.M., Churikova, T.G., Dorendorf, F., Woerner, G., Volynets, O.N., 2001. Geochemical evidence for the melting of subducting oceanic lithosphere at plate edges. Nature 409, 500-504.

Table 1: Summary of zircon U-Pb ages and Hf isotopes.

Sample	Age type	Age (Ma)	2σ (Ma)	n	Interpre-tation	εHf_i	2σ
07A1	Concordia	979	5	15	igneous		
	$^{207}Pb/^{206}Pb$ wtd. av.	987	13				
07C1	Concordia	986	3	18	igneous		
	$^{207}Pb/^{206}Pb$ wtd. av.	987	6				
12B4	Concordia	984	6	12	igneous		
	$^{207}Pb/^{206}Pb$ wtd. av.	994	8				
	Upper intercept	1024	14	4	inherited		
	$^{207}Pb/^{206}Pb$ wtd. av.	1039	13				
28B2	Concordia	991	5	11	igneous		
	$^{207}Pb/^{206}Pb$ wtd. av.	990	6				
MESR99	Concordia	1015	4	20	igneous	+6.5	2.6
	$^{207}Pb/^{206}Pb$ wtd. av.	1010	5				
MESR43	Concordia	991	4	25	igneous	+6.5	2.0
	$^{207}Pb/^{206}Pb$ wtd. av.	986	4				
MESR104	Concordia	986	6	14	igneous	+6.3	1.7
	$^{207}Pb/^{206}Pb$ wtd. av.	984	7				
MESR79	Concordia	986	7	15	igneous	+7.3	2.4
	$^{207}Pb/^{206}Pb$ wtd. av.	990	18				
MESR110	Upper intercept	979	18	8	igneous	+4.2	1.2
	$^{207}Pb/^{206}Pb$ wtd. av.	979	15				
MESR106	Concordia	957	8	11	igneous	+7.5	2.1
	$^{207}Pb/^{206}Pb$ wtd. av.	957	5				
	$^{207}Pb/^{206}Pb$	1006-1070		4	inherited	+7.9	0.8
	$^{207}Pb/^{206}Pb$	2910-2966		1	inherited?	+3.6	0.9
MESR49a	Concordia	947	8	10	igneous	+7.7	1.8
	$^{207}Pb/^{206}Pb$ wtd. av.	960	7				
MESR109	Upper intercept	927	+37 -22	2	igneous	+6.9	5.2
	$^{207}Pb/^{206}Pb$ wtd. av.	929	14				
	Upper intercept (with MESR106)	2970	+32 -30	1	inherited	-2.1	

n = number of analyses on which the age is based
Samples 07A1, 07C1, 12B4 and 28B2 analysed by SHRIMP, others by LA-MC-ICPMS.

Table 1: Representative whole rock analyses

Sample name	MESR-43	MESR-49A	MESR-79	MESR-99	MESR-104	MESR-106	MESR-109	MESR-110
	Widerøe-fjellet C	Lag-kollane	Bamse ungen	Widerøe-fjellet E	Nils Larsen-fjellet W	Widerøe-fjellet SE	Causin-knappen	Causin-knappen
SiO_2	73.70	66.01	74.66	79.85	68.34	72.59	48.43	63.77
TiO_2	0.19	0.55	0.28	0.06	0.40	0.19	3.67	0.39
Al_2O_3	12.43	15.97	13.54	11.70	14.54	14.87	12.39	15.30
$Fe_2O_3^*$	3.57	4.61	2.85	0.85	6.25	2.22	17.18	7.67
MnO	0.08	0.11	0.03	0.02	0.15	0.05	0.27	0.16
MgO	0.51	0.73	0.83	0.22	1.26	0.58	4.80	1.84
CaO	3.97	2.92	1.86	3.22	5.71	3.12	8.93	8.41
Na_2O	3.31	6.25	5.50	3.66	2.27	4.17	2.21	0.90
K_2O	0.69	1.66	0.53	0.16	0.20	1.09	0.31	0.13
P_2O_5	0.05	0.11	0.05	0.02	0.12	0.04	0.60	0.15
LOI	1.05	0.45	1.59	0.73	1.36	1.18	0.36	0.31
Sum	98.59	99.14	100.22	99.83	99.29	99.02	99.33	98.81
Sc	11	9	9	5	17	4	46	27
V	30	19	16	7	60	19	475	132
Zn	45	83	26	7	62	34	128	70
Ga	12	24	17	10	15	15	25	13
LA-ICPMS								
Rb	18.3	52.3	11.0	3.1	6.8	24.9	2.7	2.6
Sr	126	381	125	134	186	433	181	231
Y	19.3	45.6	44.6	4.1	8.6	9.9	53.4	5.5
Zr	66.9	567	169.2	203.5	19.1	87.4	128.1	11.9
Nb	2.3	19.6	4.1	0.3	0.7	5.5	3.6	0.7
Cs	1.0	1.9	0.5	0.2	0.3	0.5	0.1	0.2
Ba	121.6	418.7	158.7	92.3	61.0	244.2	69.4	27.7
La	10.5	36.6	12.5	3.6	2.1	6.2	6.7	2.5
Ce	17.9	72.8	29.0	6.2	5.8	10.8	16.1	10.1
Pr	3.0	10.8	3.9	0.7	0.9	1.3	2.9	1.0
Nd	12.9	44.5	17.5	2.9	4.0	5.2	17.2	4.4
Sm	3.0	9.5	4.7	0.6	1.3	1.2	6.1	1.3
Eu	0.63	2.08	0.92	0.67	0.68	0.64	2.17	0.46
Gd	2.79	8.30	5.74	0.61	1.47	1.57	8.32	1.18
Tb	0.48	1.30	0.97	0.11	0.25	0.29	1.41	0.20
Dy	3.24	8.33	7.68	0.60	1.58	1.58	9.73	1.10
Ho	0.69	1.69	1.54	0.16	0.33	0.37	2.09	0.26
Er	2.11	4.84	4.81	0.55	0.86	1.00	5.77	0.69
Tm	0.33	0.77	0.79	0.11	0.13	0.20	0.87	0.12
Yb	2.31	5.08	5.55	0.83	0.96	1.13	5.65	0.69
Lu	0.35	0.79	0.81	0.16	0.15	0.21	0.86	0.14
Hf	2.21	13.88	5.01	5.47	0.57	2.36	3.84	0.44
Ta	0.19	1.09	0.32	0.04	0.05	0.63	0.31	0.08
Pb	8.22	13.42	3.72	4.79	1.76	15.13	1.89	4.56
Th	2.21	5.51	3.11	0.62	0.52	2.08	1.16	0.76
U	1.06	2.61	1.45	1.01	0.24	0.75	1.00	0.47
$^{87}Sr/^{86}Sr$	0.708200					0.705215		
2se	0.000012					0.000012		
$^{87}Rb/^{86}Sr$	0.3489					0.1289		
$^{87}Sr/^{86}Sr_i$	0.703256					0.703452		
εSr_i	-1.25					0.97		
$^{143}Nd/^{144}Nd$	0.512412					0.512588		
2se	.000009					.000012		
$^{147}Sm/^{144}Nd$	0.1364					0.1577		
$^{143}Nd/^{144}Nd_i$	0.511525					0.511598		
εNd_i	3.24					3.81		

LOI = Loss on Ignition. $Fe_2O_3^*$ = all Fe as Fe_2O_3.

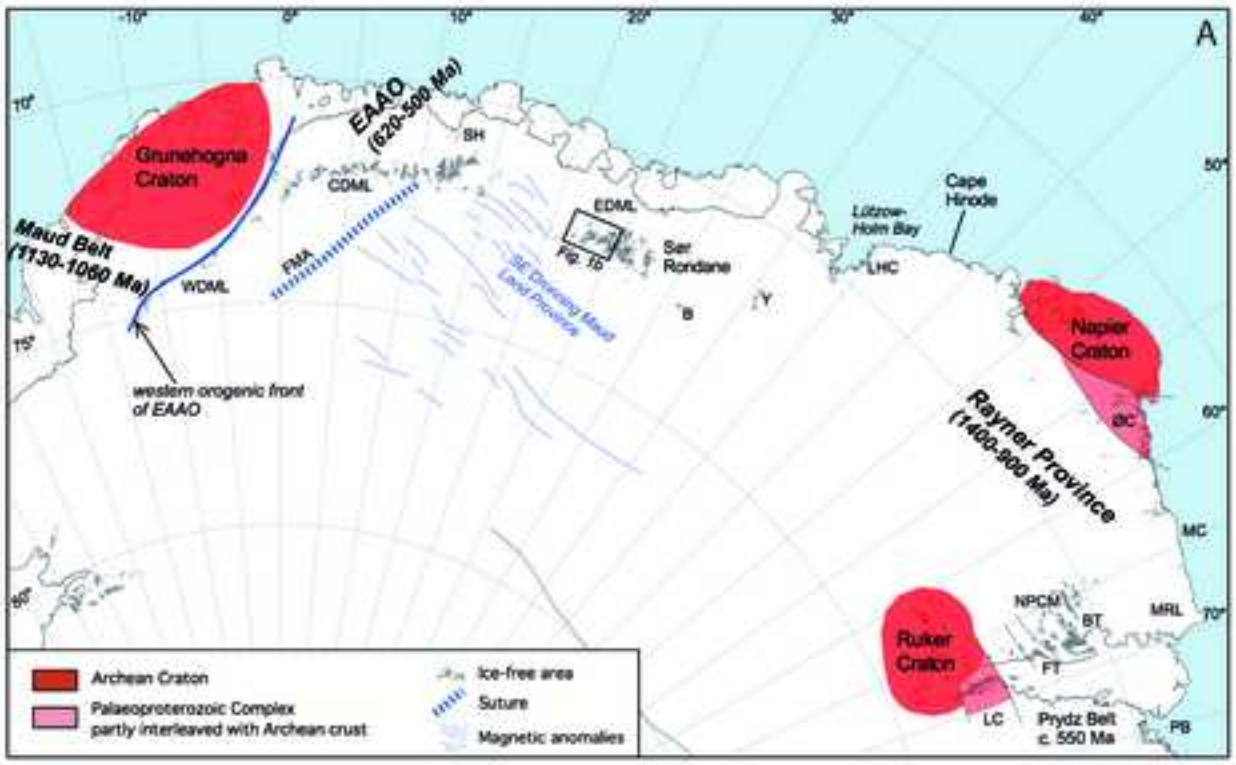

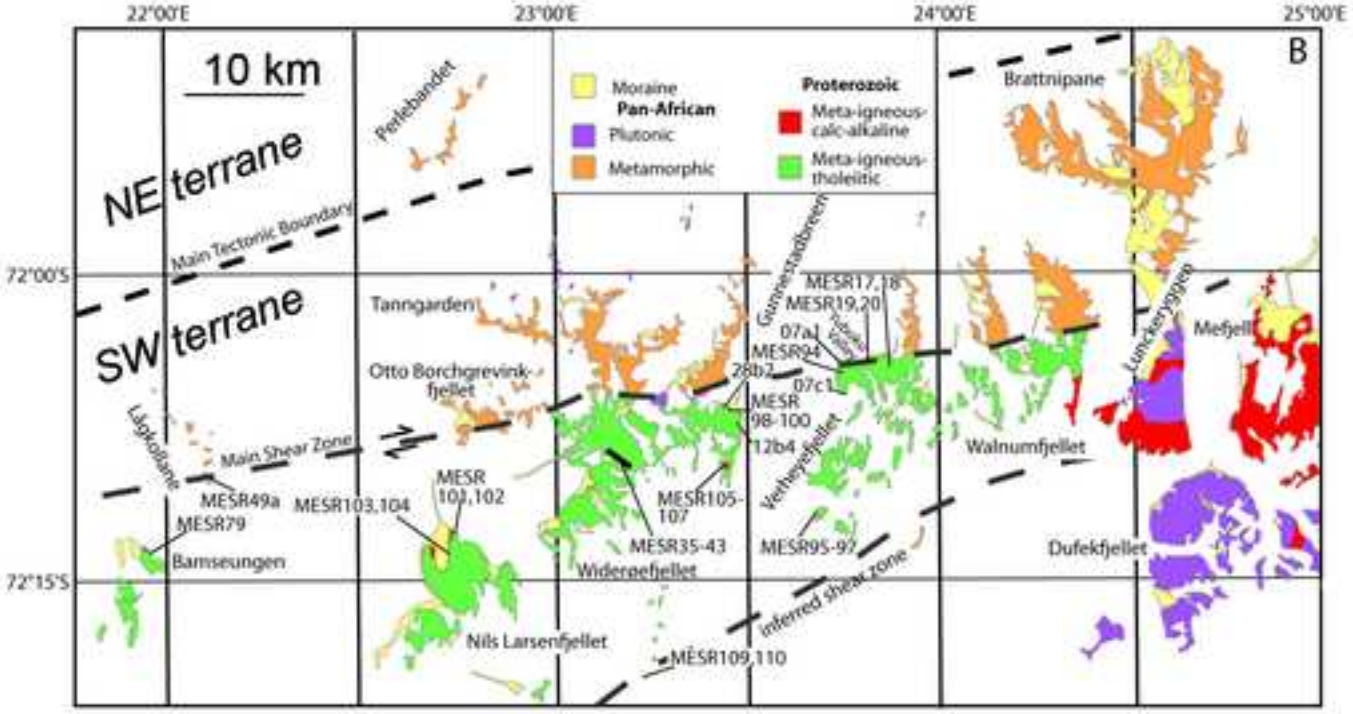

Fig. 1

Figure 3

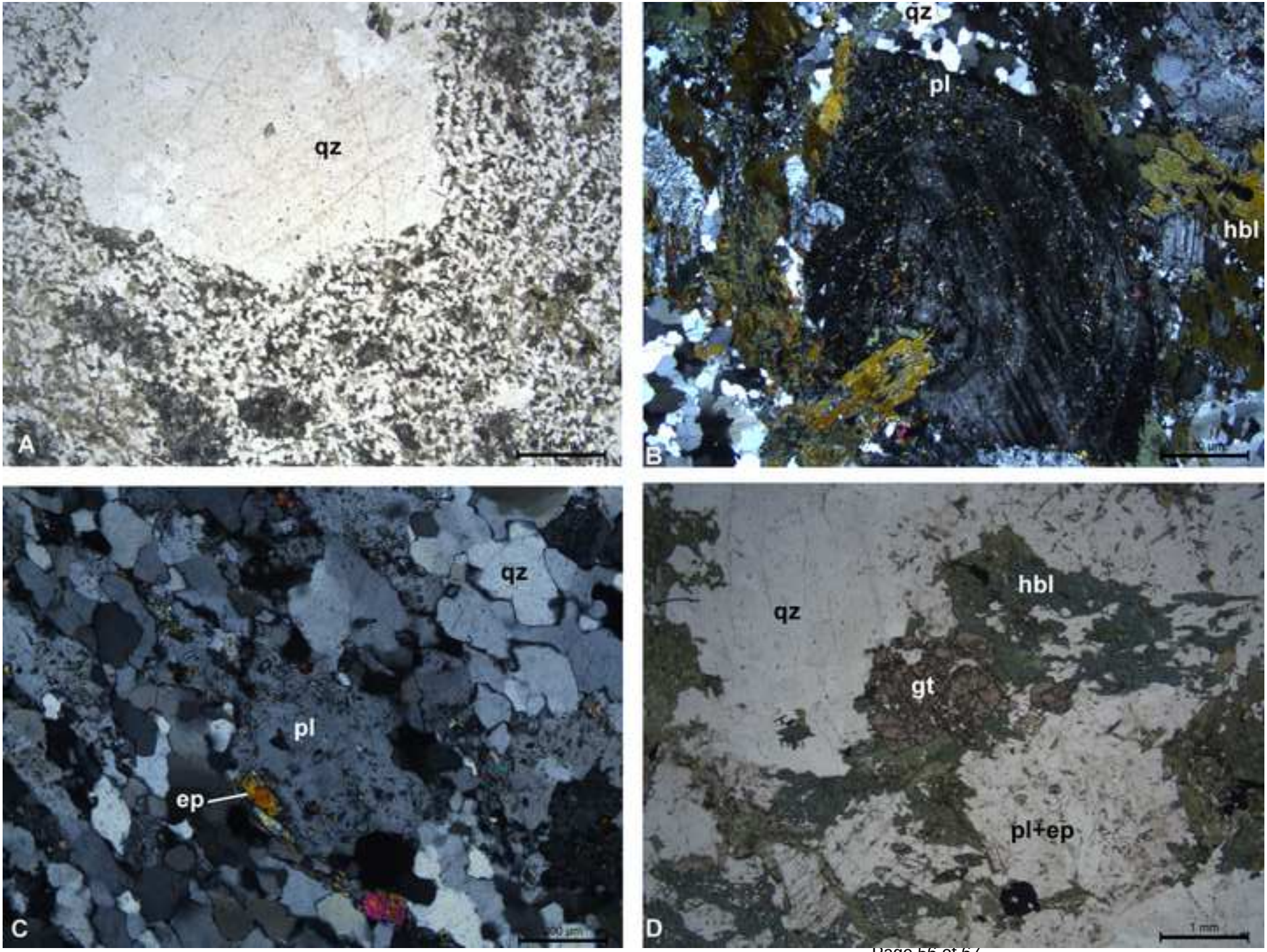

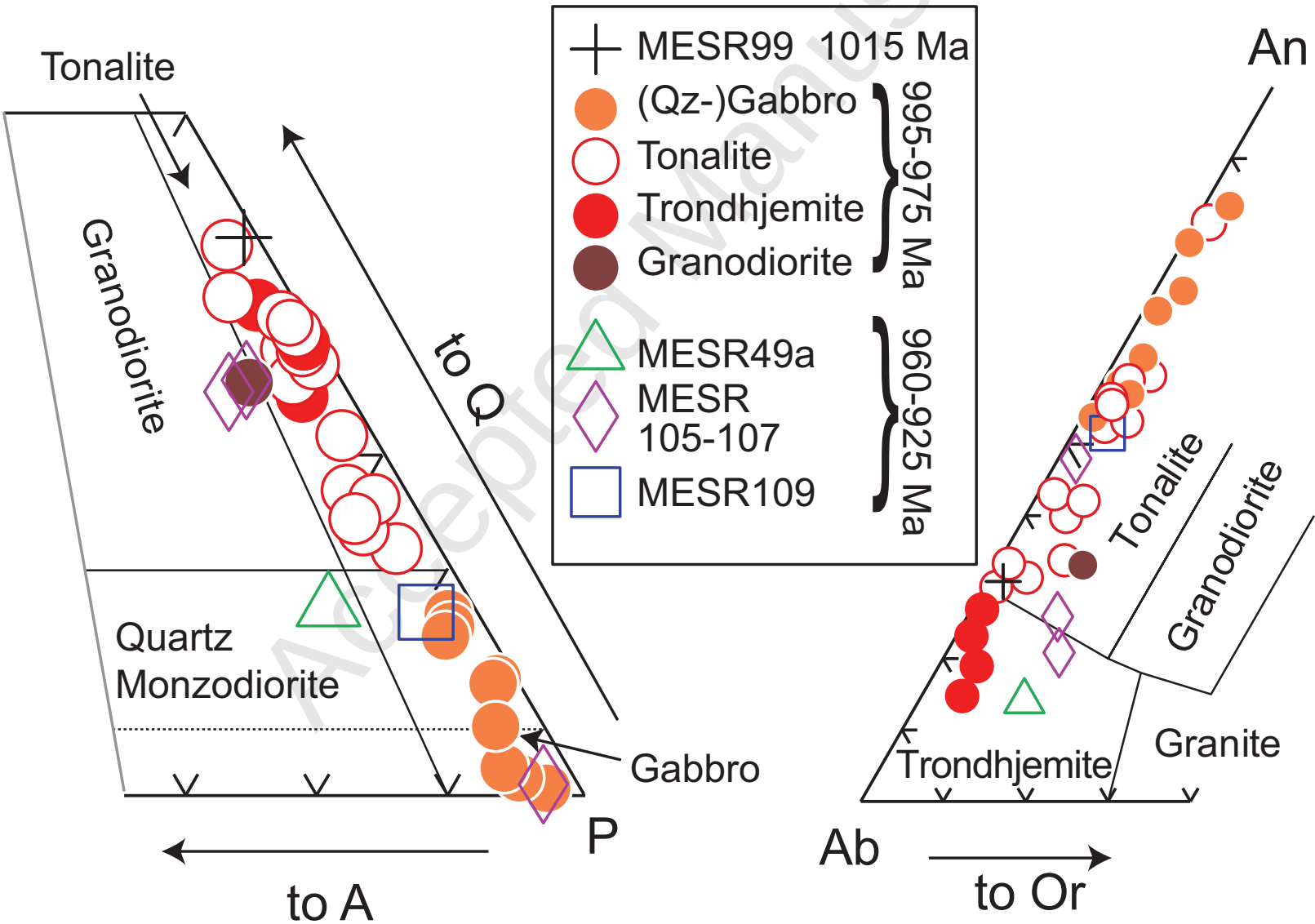

Fig. 4 Elburg et al.

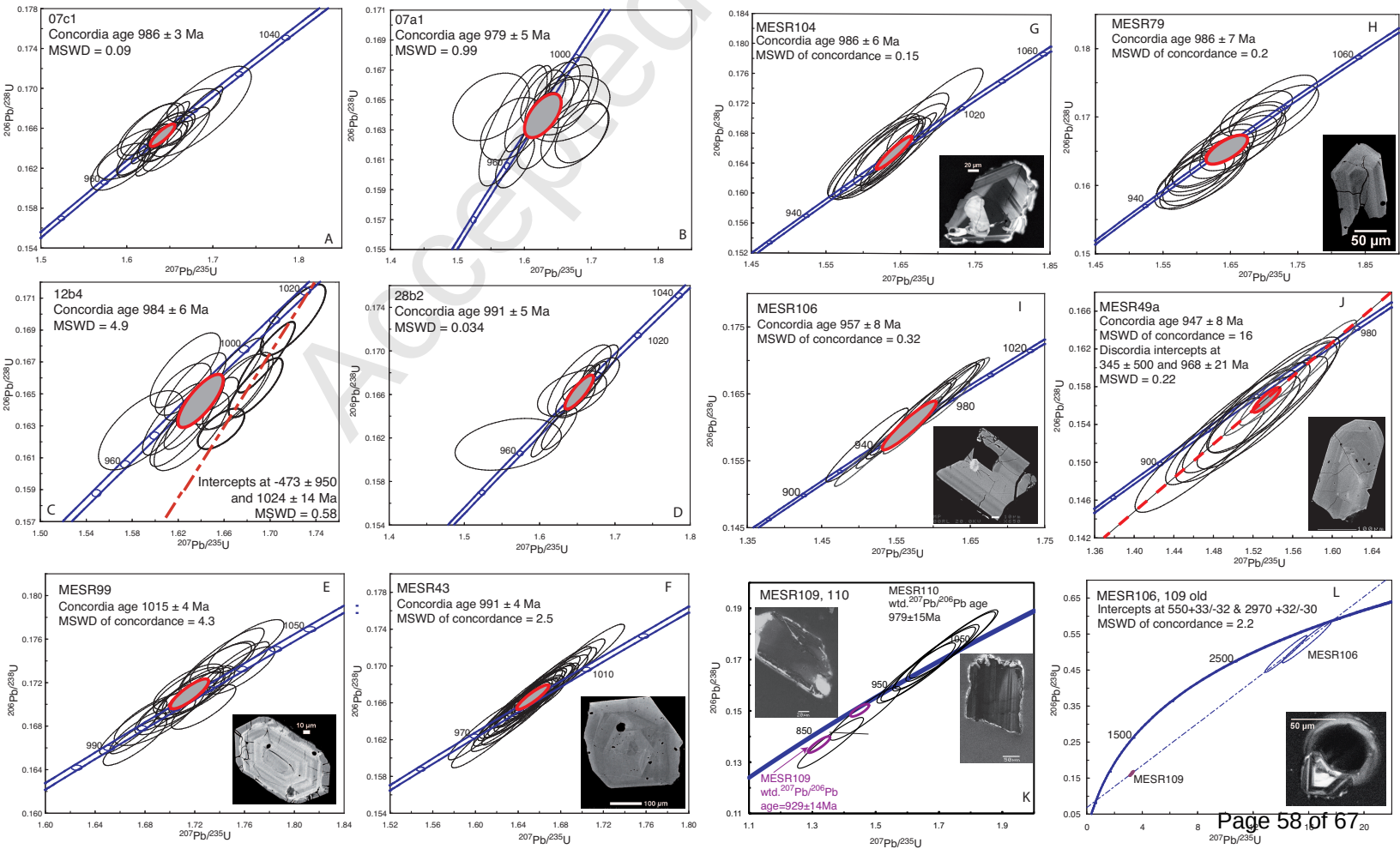

Fig. 5

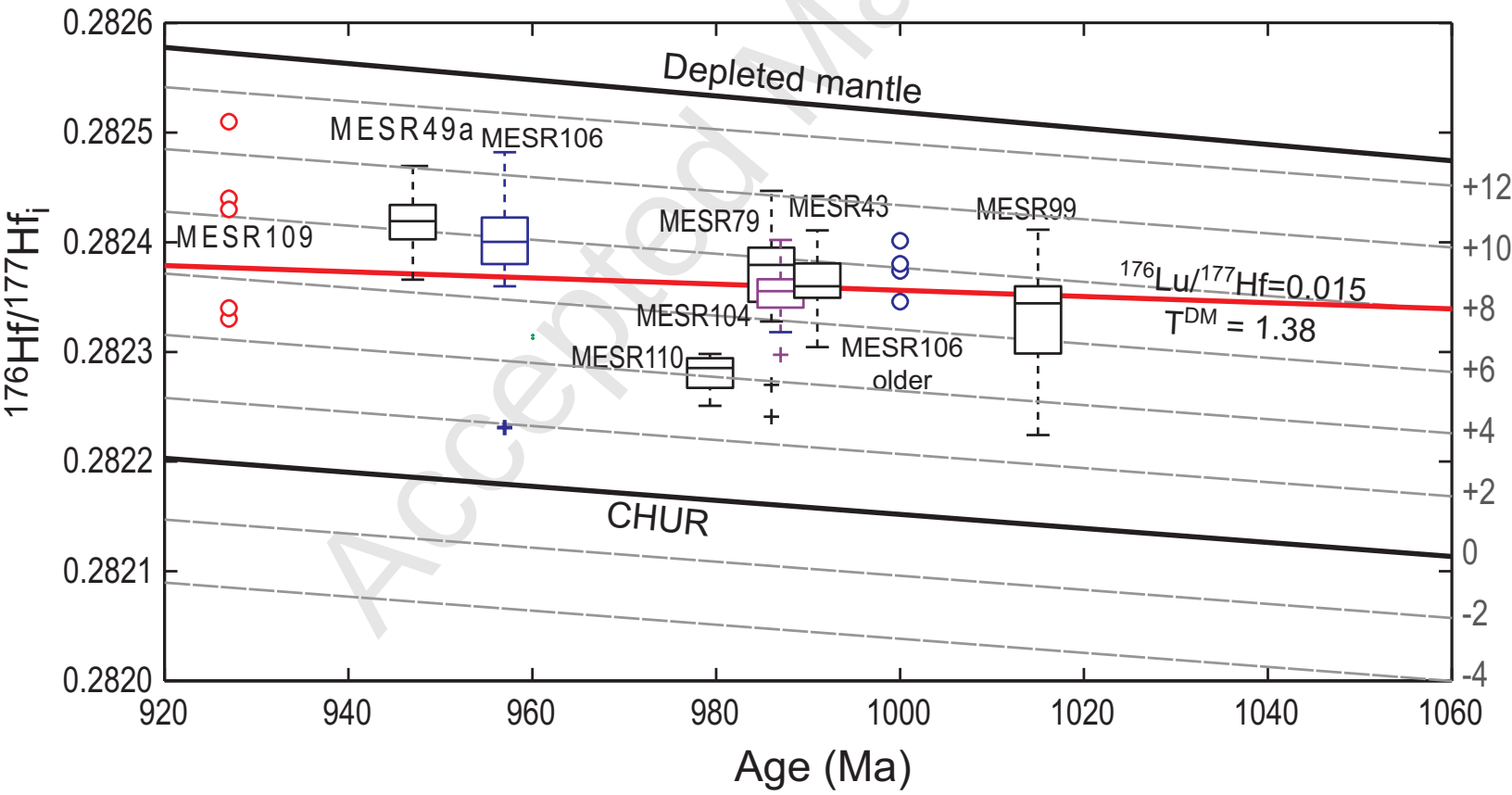

Fig. 6 Elburg et al.

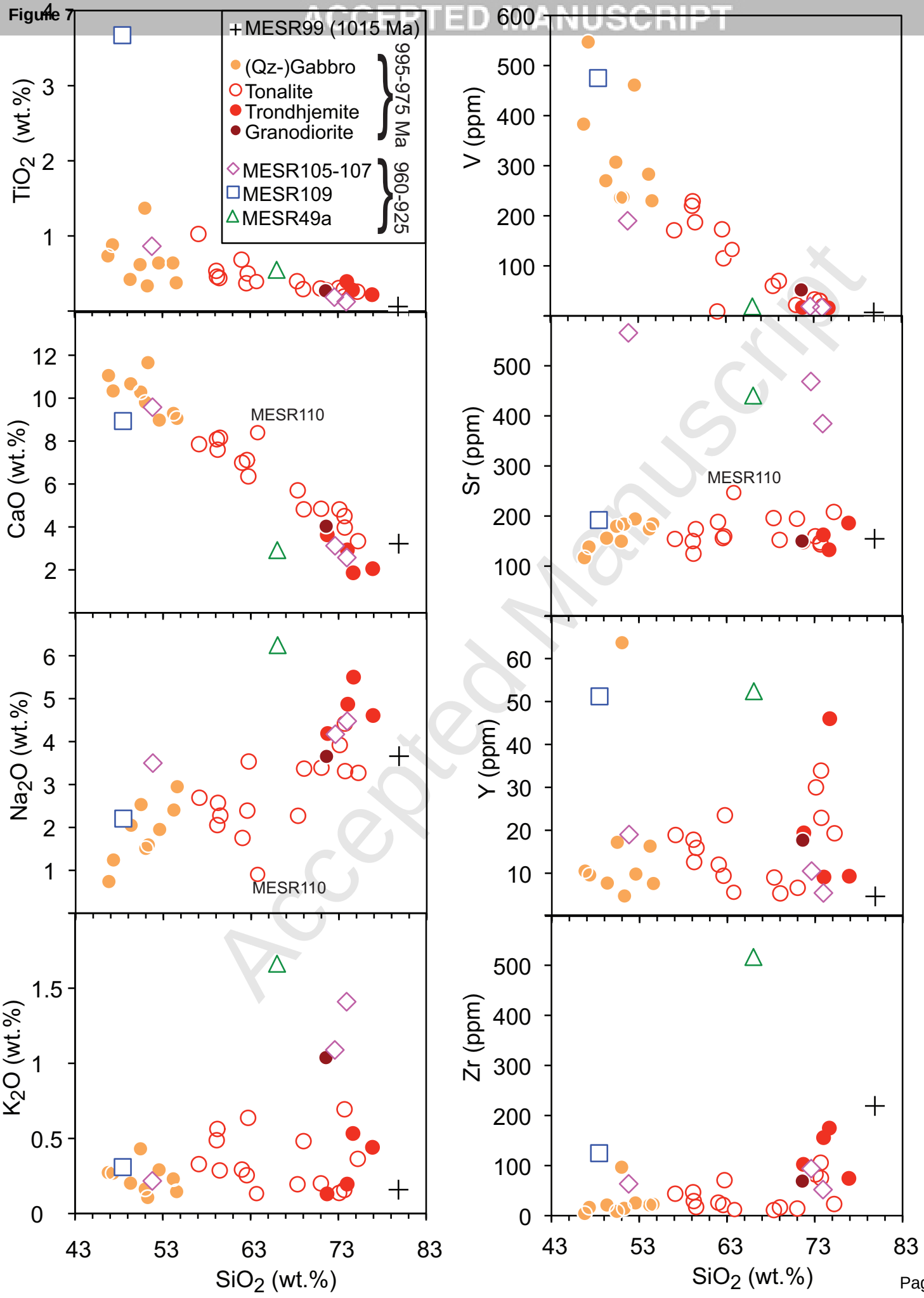

Fig. 7 Elburg et al.

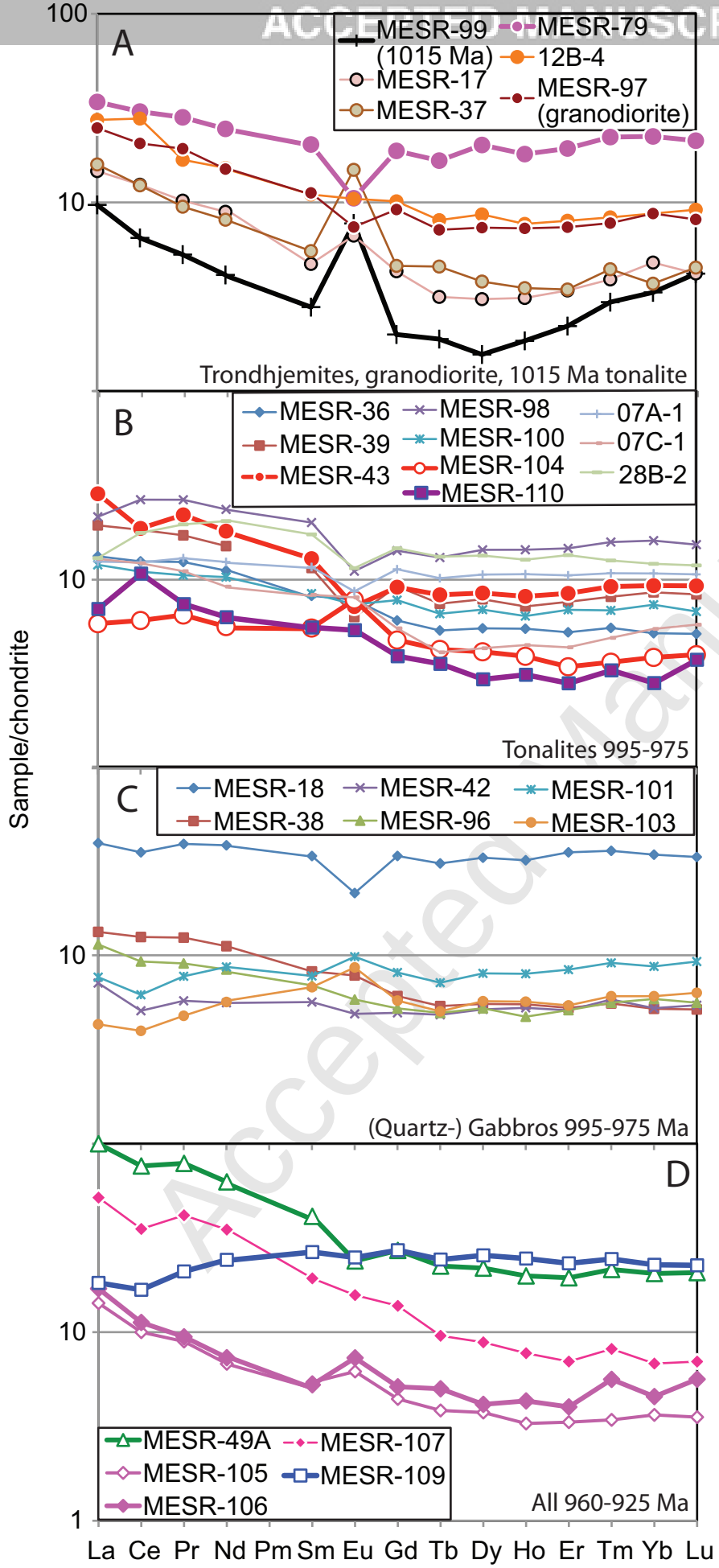

Fig. 8 Elburg et al.

Figure 9

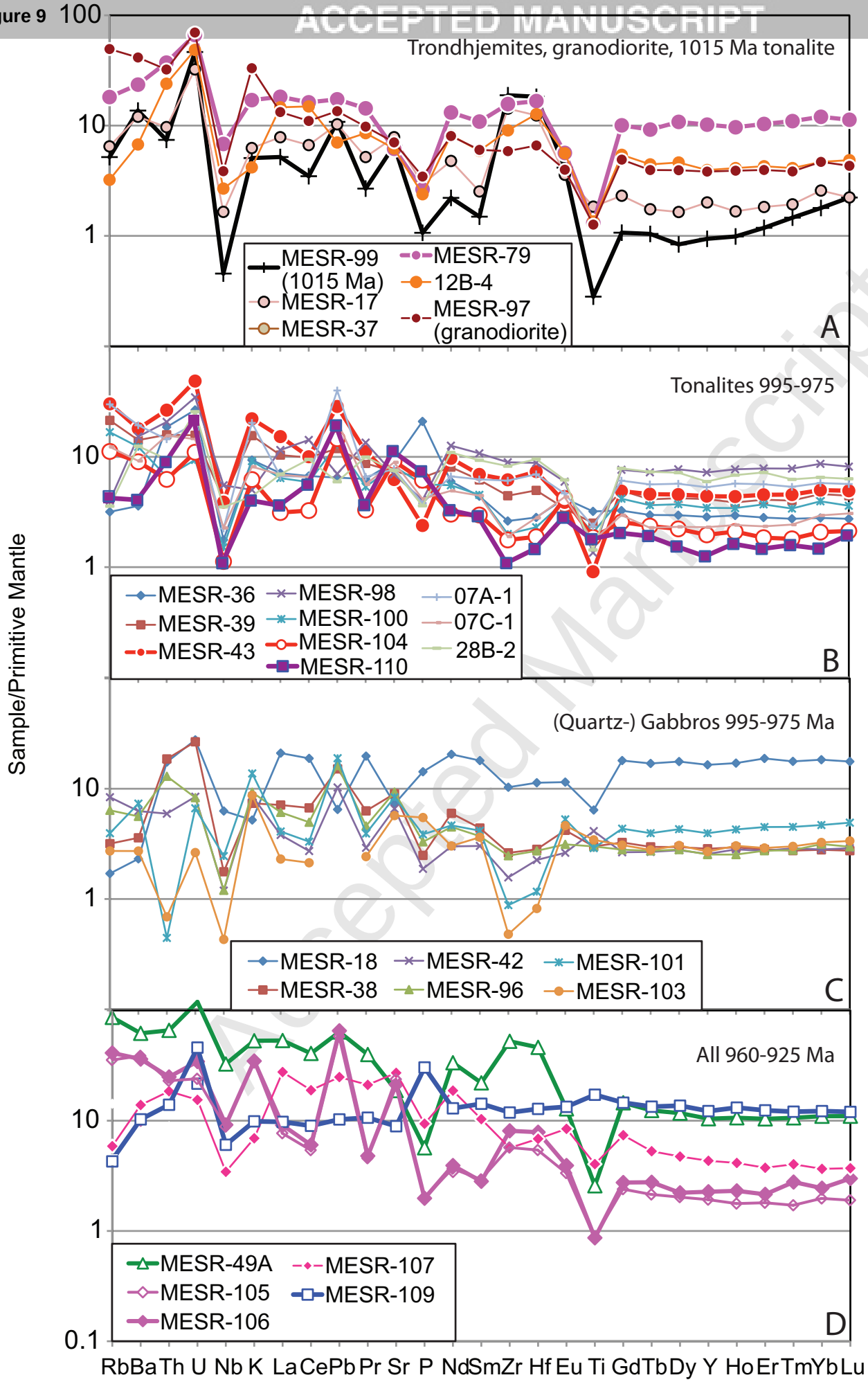

Fig. 9 Elburg et al.

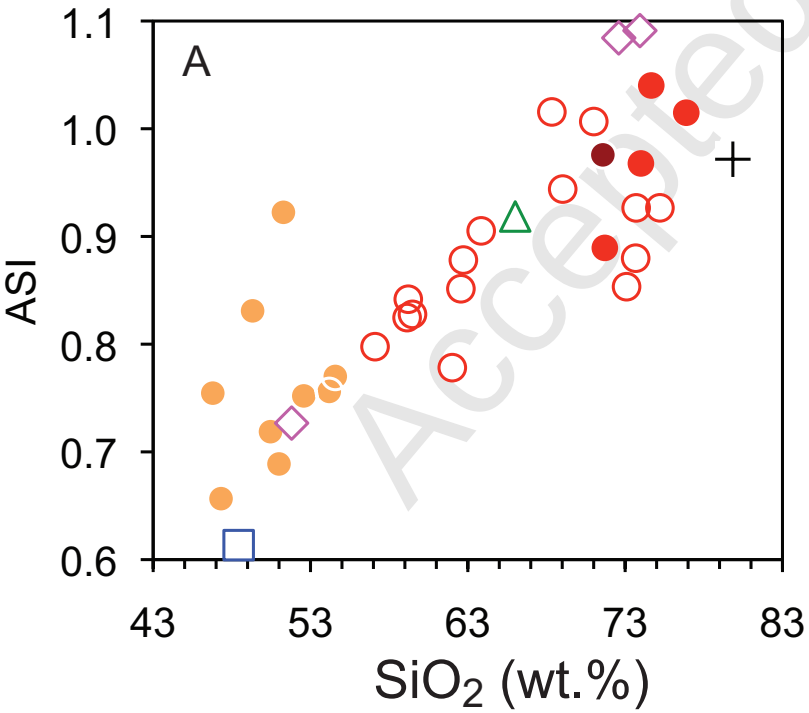

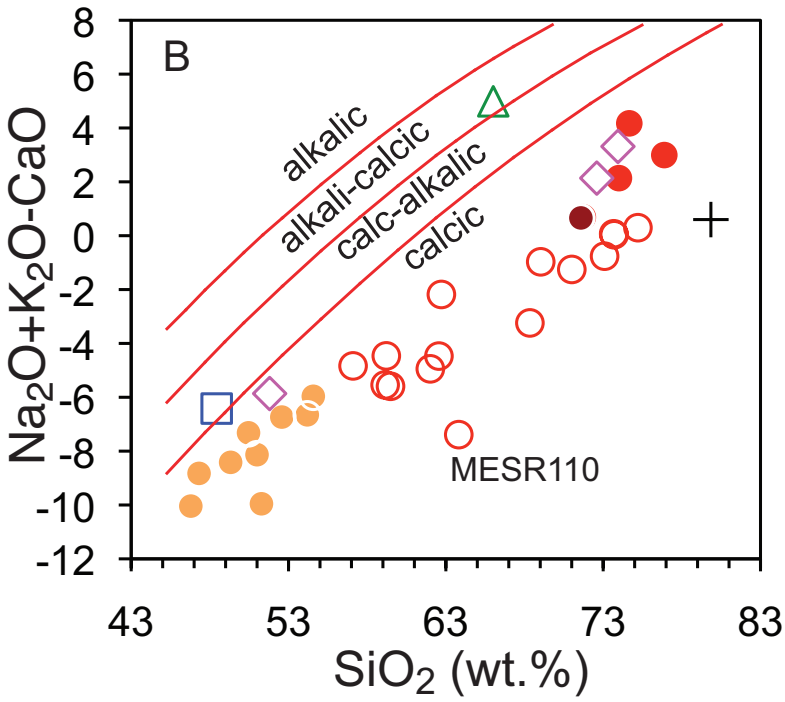

Fig. 10 Elburg et al.

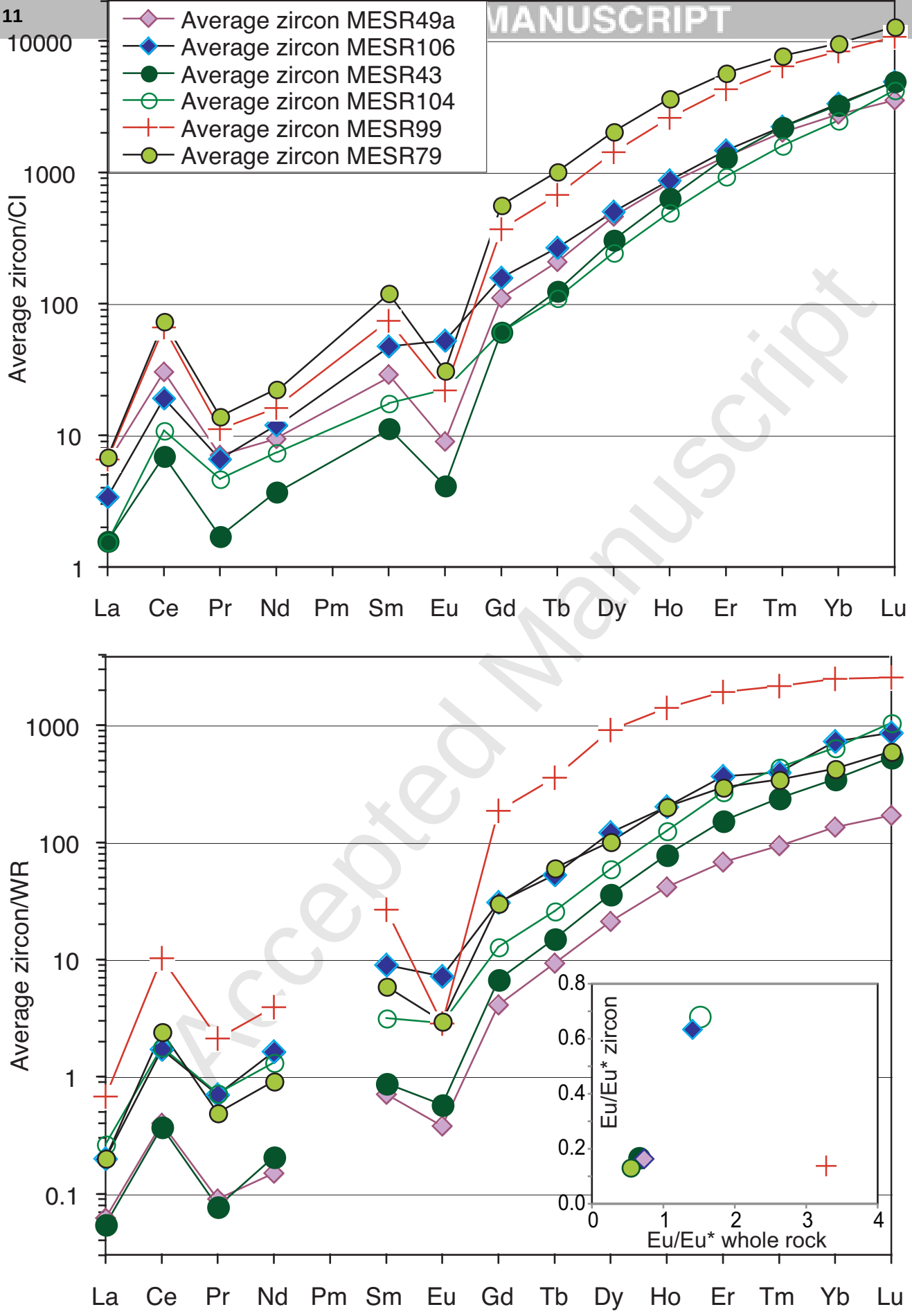

Fig. 11

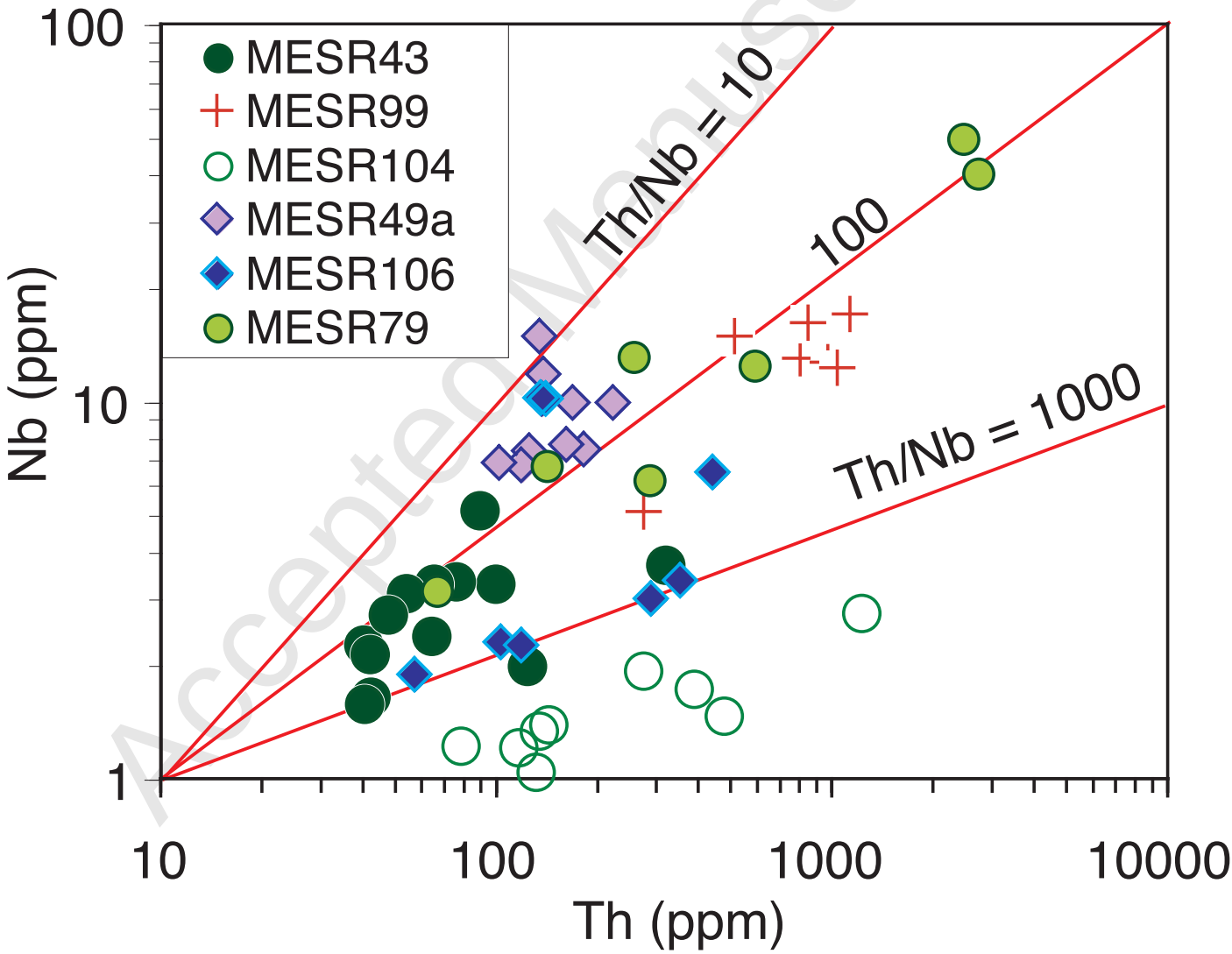

Fig. 12

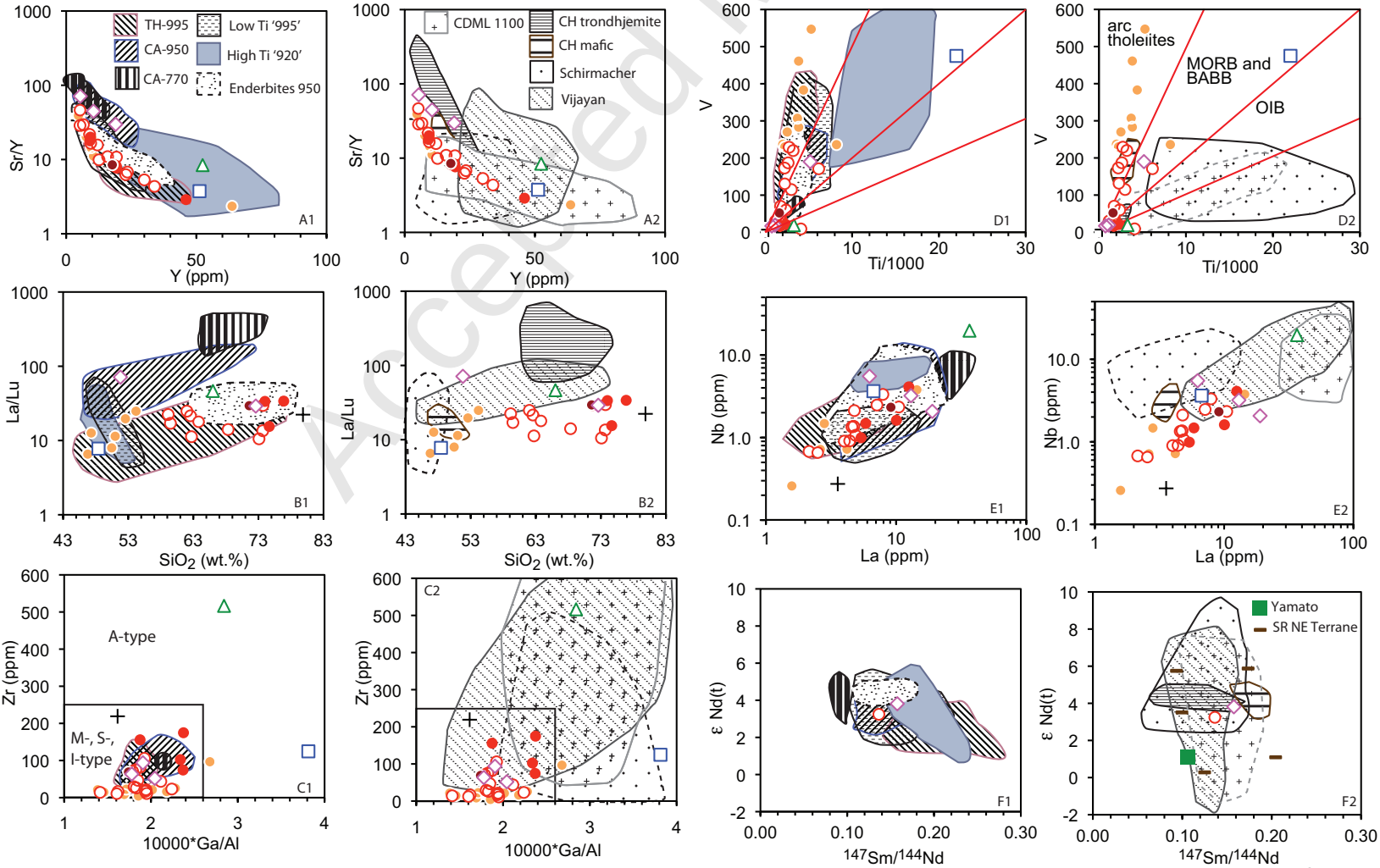

Fig. 13 Elburg et al.

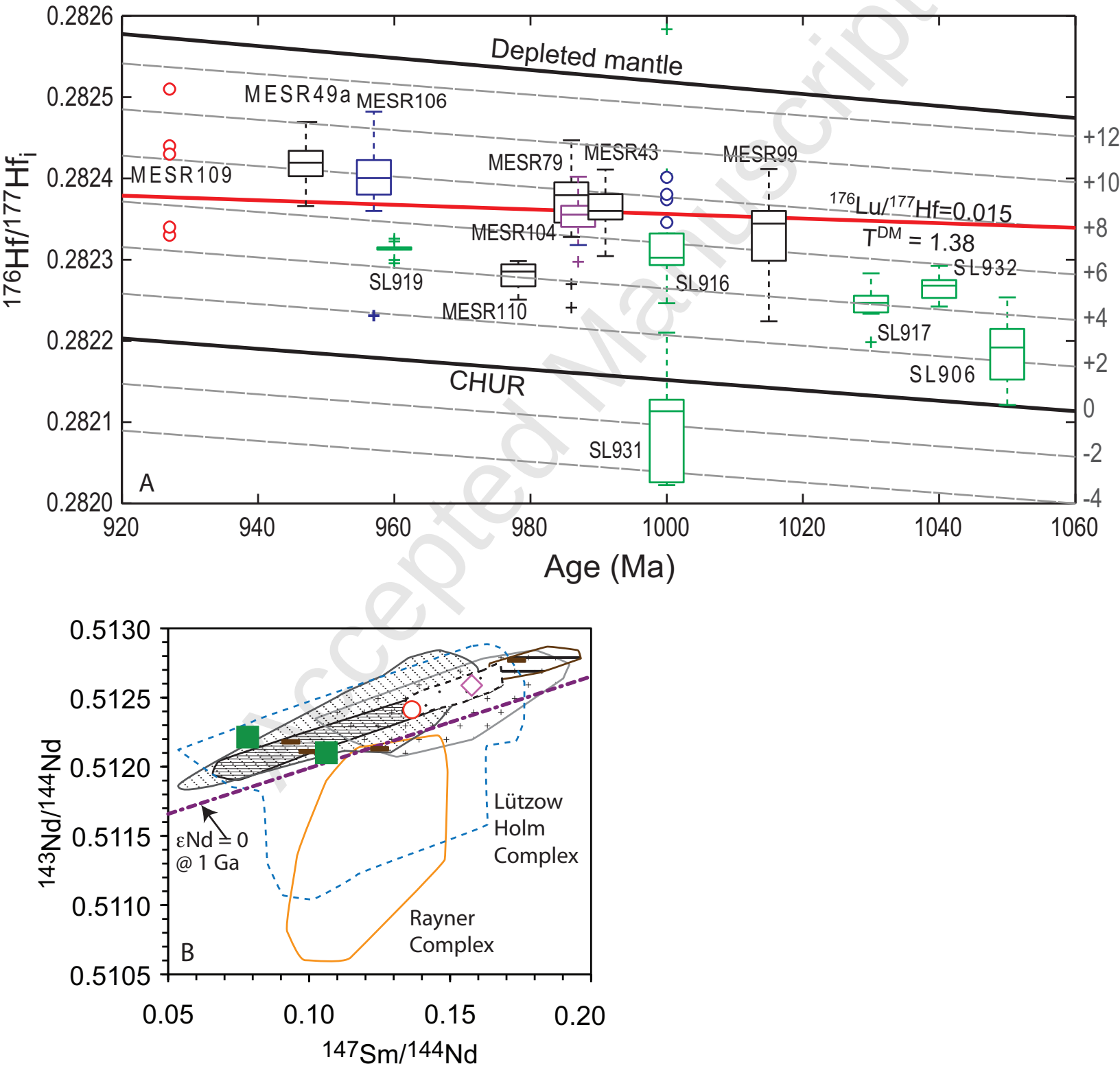

Fig. 14 Elburg et al.